Electroencephalographic Microstate Correlates of Fluid Intelligence

ABSTRACT

Note: Portions of this section have been submitted for publication as:
Santarnecchi E, Khanna AR, Museus C, Benwell C, Davila P, Pascual-Leone A, Shafi MM. EEG microstate correlates of fluid intelligence. Proceedings of the National Academy of Science (Submitted, under review); 2016.

The neurobiological correlates of human fluid intelligence (*Gf*) remain elusive. Converging lines of evidence suggest a pivotal role for the efficiency and connectivity of anatomically-defined brain networks, but little is known about *Gf*-related electrophysiological dynamics of these networks occurring at native timescales, such as those measured via electroencephalography (EEG). Spatiotemporal analysis of state-space dynamics of the EEG signal, involving examination of fast-changing, recurring, topographically-defined electric patterns termed “microstates,” may enable investigation of the electrophysiological activity of distributed cortical networks and their relation to brain characteristics, including *Gf*. Here, we correlated EEG microstate patterns with multiple fluid intelligence measures, and assessed changes in microstate patterns after cognitive training aimed at improving intelligence. We found that the frequency of activation of specific brain topographies, spatially associated with visual (microstate B) and executive control (microstate C) networks, were inversely related to *Gf* scores. When *Gf* scores were separated into two distinct “dimensions” of intelligence using latent factor analysis, each “dimension” correlated with a different microstate, suggesting that each microstate class represents a distinct cognitive modality. Cognitive training resulted in a posterior shift in the topography of microstate C, possibly reflecting increased prefrontal inhibitory control over parietal brain regions. These results highlight the role of fast-changing brain electrical states related to visual and executive functions in *Gf*, as well as the mechanisms behind *Gf* enhancement after cognitive training.

TABLE OF CONTENTS

ACKNOWLEDGMENTS

I would like to extend my deepest gratitude to my advisor, Dr. Alvaro Pascual-Leone, for his constant support and mentorship over the last four years throughout this endeavor. I also thank Dr. Mouhsin Shafi and Dr. Emiliano Santarnecchi for their guidance, collaboration, and invaluable teaching during the course of this project. I owe special thanks to Dr. Faranak Farzan for providing the initial inspiration to study spatiotemporal EEG analysis.

I thank the Harvard Medical School Scholars in Medicine program for its funding support of portions of my work over the last several years, and for constant academic guidance.

Finally, I am indebted to the Intelligence Advanced Research Projects Activity (IARPA) and their establishment of the Strengthening Human Adaptive Reasoning and Problem-Solving (SHARP) program for funding of the project described in this work.

GLOSSARY OF ABBREVIATIONS

BOMAT	Bochumer Matrizentest
EEG	Electroencephalography
ERD	Event related desynchronization
fMRI	Functional magnetic resonance imaging
g	General factor (general intelligence)
Gf	Fluid intelligence
Gc	Crystallized intelligence
IQ	Intelligence quotient
MEG	Magnetoencephalography
P-FIT	Parieto-frontal integration theory
RAPM	Raven's advanced progressive matrices
RSN	Resting-state network
tACS	Transcranial alternating current stimulation

I. INTRODUCTION

Note: Portions of this section appeared in the following published work, and is reproduced here in accordance with the content license agreement with the publisher:
Khanna A, Pascual-Leone A, Farzan F. Reliability of resting-state microstate features in electroencephalography. PLoS One. Public Library of Science; 2014;9(12):e114163.

Note: Portions of this section have been submitted for publication as:
Santarnecchi E, Khanna AR, Museus C, Benwell C, Davila P, Pascual-Leone A, Shafi MM. EEG microstate correlates of fluid intelligence. Proceedings of the National Academy of Science (Submitted, under review); 2016.

Formulation of human intelligence: G*,* Gf*, and* Gc

In 1904, Charles Spearman observed that the performance of schoolchildren on a variety of school performance measures, including French and English grammar, mathematics, Classics, pitch discrimination, and musical ability, were all positively correlated with each other – far beyond what would be expected if each measure involved an independent component of mental ability (1). He hypothesized that these measures constituted a "Hierarchy of Intelligences," atop which was a factor termed "General Intelligence," or *g*, which was an intrinsic feature of each child's overall intellectual ability and explained the high degree of correlation among performances on seemingly disparate tasks. The *g* factor quantifies the degree of correlation among such tests, and aims to measure the degree of overall intellectual ability of each subject. This finding – of positive correlation among mental test scores, despite large variation in test content – has been repeatedly observed in studies of different populations, age groups, test types, difficulty levels, and time constraints (2,3). Indeed, this autocorrelation has been called "arguably the most replicated result in all psychology" (4).

Catell and Horn subsequently modified Spearman's formulation of *g* by suggesting that *g* was separable into two factors, termed crystallized intelligence (*Gc*) and fluid intelligence (*Gf*). Crystallized intelligence is a knowledge-based component that refers to abilities accrued across one's lifespan through education and experience. Tests of *Gc* broadly involve challenges of information retention, organization, and retrieval. In contrast, fluid intelligence refers to the ability to think abstractly, solve novel problems, apply logical and probabilistic reasoning, and learn – skills with a "fluid quality of being directable to almost any problem" (5). Fluid and crystallized intelligence are correlated (6). Some authors have taken this correlation to suggest a higher-level construct of *g*, of which *Gc* and *Gf* are components (7), while others have argued that *g* is a statistical artifact, perhaps arising from imperfections in tests used to measure *Gf* and *Gc*, and that *g* holds limited neuropsychological relevance (8). Catell proposed an "Investment Theory," in which individuals "invest" fixed amounts of *Gf* into acquiring *Gc* (5,9). Despite debate on the nature of their relationship, the distinction between *Gc* and *Gf* as separate constructs of human intelligence is widely accepted.

While *Gc* can be increased with schooling, study, experience, and other means of information acquisition, *Gf* seems to be less mutable. The rank order of performance on general intelligence tests loading on *Gf*-related components remains remarkably stable over time. For example, a study of repeated intelligence quotient (IQ) testing using the revised Wechsler Intelligence Scale for Children (WISC-R) on 794 children at age 7, 9, 11, and 13 concluded that there was very little naturalistic change in IQ from ages 7-13, and that idiosyncratic, unpredictable factors were responsible for the minority of cases in which students exhibited significant improvements in IQ (10). Another longitudinal study found that scores on a general intelligence test taken at ages 11 and 79 had an estimated correlation of 0.73, suggesting a high degree of stability over the entire lifespan (11). Moreover, *Gf* is highly heritable, suggesting a physiologic basis for individual differences in *Gf* and its stability over time (12,13).

Despite this apparent stability, the idea of *Gf* as a stable and immutable cognitive characteristic has been recently challenged by studies demonstrating enhancement of *Gf* in healthy individuals following external interventions. This was vividly demonstrated by Jaeggi et al., who showed that cognitive training with a demanding working memory task over 8-19 days resulted in performance improvement on different tests of *Gf* in a dose-dependent manner with respect to amount of training (14). A later meta-analysis of 20 studies showed that training using an *n*-back program produced small but significant improvements in *Gf* (15). In addition to cognitive training paradigms, a few studies have demonstrated that application of transcranial alternating current stimulation (tACS) is also capable of transiently improving *Gf*. This was first shown by Santarnecchi et al., who applied γ-frequency tACS over the left middle frontal gyrus that resulted in shortening of time required to find the correct solution in a visuospatial abstract reasoning task used to measure *Gf* (16,17). Another group showed that θ-frequency tACS over left frontal and left parietal areas resulted in similar improvements, with greater improvements observed after left parietal *vs* frontal stimulation (18). Together, these reports indicate a highly dynamic neurophysiological component of *Gf*, and enable study of dynamic brain rearrangement following external "perturbation" eliciting an increase in performance (see below).

There is considerable interest in understanding the basis of individual differences in *g*, and in particular *Gf*. This is because *Gf* is correlated with several socioeconomic factors, such as academic achievement and occupational success. Intriguingly, there is a robust association between *Gf* and longevity (19). For example, in a systematic review of 9 studies in which early life IQ was compared to mortality, all 9 studies showed that mortality increased in groups with lower IQ; belonging to the lowest quartile of IQ compared to the highest quartile was associated with between 50-100% increased risk of death (20).[1] Moreover, *Gf* usually declines with age and in many neurodegenerative disorders, which plays a key role in the dramatic functional impairment of many chronic-degenerative neurological conditions (21). Thus, a greater understanding of the basis of differences and changes in *Gf* has widespread relevance for aging, education, neuropsychiatric disease, socioeconomic health disparities, and more.

Neurobiology of Gf*: Convergence toward P-FIT theory*

The neurobiological basis of *Gf* is one of the most enduring and elusive questions in modern psychology and neuroscience. Over more than two centuries of research into this question, two schools of thought emerged: one suggesting that the entire brain functions as a single entity, from which higher cognitive function, including intelligence, emerges; and another proposing that discrete cortical regions are independently responsible for different cognitive facilities. These ideas were integrated by Pavlov, who first suggested that higher cognitive function was due to interactions between distributed cortical loci – an idea that has persisted to the present day. This concept has guided modern neuroanatomical and neuroimaging studies of *Gf*, in which the activity of specific cortical loci – or the functional interaction between them – are studied in relation to intelligence.

[1] Some have argued that the association between intelligence and mortality is confounded by socioeconomic status; specifically, that intelligence is associated with more education, which may ultimately place individuals of higher intelligence into healthier environments. Statistical adjustment for socioeconomic status does lessen or eliminate the association between intelligence and mortality, but not consistently (20). Furthermore, the direction of causality between intelligence and education/environment is unclear; while individuals with more education may achieve higher IQ, it may also be true that higher IQ makes an individual more likely to undergo more education. Indeed, one provocative paper has suggested that variance in intelligence is the "fundamental cause" of the association between socioeconomic status and health disparities (105).

There is now a large and rapidly growing body of neuroanatomical and neuroimaging literature on the subject of the neurobiological bases of *Gf*. Recently, Jung & Haier (2007) conducted a comprehensive review of all modern neuroimaging studies and identified convergence among these studies toward a central role for discrete parieto-frontal networks in human intelligence (22). Their proposed "Parieto-Frontal Integration Theory" (P-FIT) involves integration of multiple distributed brain regions into large-scale networks that involve a variety of tasks, including perception and early processing of visual and auditory information (extrastriate cortex, fusiform gyrus, and Wernicke's area), abstraction and elaboration of input (supramarginal, superior parietal, and angular gyri), solution generation and testing (frontal cortex), and suppression of competing responses (anterior cingulate cortex), all of which requires intact white matter tract to pass information among these distributed loci. Although the P-FIT theory has been challenged, it nevertheless is recognized as a reasonable model roughly consistent with existing neuroimaging data, and provides a valuable framework for the generation and testing of future hypotheses.

Notably, Jung & Haier did not include EEG or magnetoencephalography (MEG) data in the formulation of P-FIT, citing difficulties with spatial localization of electric sources for these techniques, but acknowledging their superiority in providing greater temporal resolution for the study of parieto-frontal networks. Indeed, although there are some reports of EEG correlates of intelligence, understanding the relationships among EEG, distributed cortical networks as identified in P-FIT, and *Gf* remains difficult.

Electroencephalographic correlates of Gf

Correlations between resting-state EEG measures and *Gf* have been reported in numerous prior studies, and have been reviewed extensively elsewhere (23). These studies have repeatedly shown that, in general, there is a positive correlation between resting-state EEG power within the α frequency bandwidth and a negative correlation between EEG power within the (lower-frequency) δ bandwidth (23,24). Interestingly, when challenged with a cognitive task, the reverse associations are observed – a large phasic decrease in α power is observed, while a large phasic increase in δ power can be observed in certain cases (25,26). This attenuation of α rhythms in response to stimulus or cognitive load has been termed "event-related desynchronization," or ERD. Interestingly, ERD evoked from visual stimuli is separable into two components, one focused over the occipital lobes in the high α range (10-12 Hz), and another over the parietal areas in the low α range (6-8 Hz) (27).

The functional interpretation of these findings is based on the hypothesized neurophysiological basis of the α rhythm itself – α oscillations measured at the scalp represent synchronized neuronal activity within a relatively large number of cortical modules over a few square centimeters (28). Thus, high resting-state α power reflects a high degree of baseline synchronization, while task-associated ERD of the α rhythm represents local desynchronization of these neural ensembles – likely representing transient activation, decreased local coherence, and increased complexity. Spatial and spectral distinction between two independent components of visual-evoked ERD may represent processing of input stimuli in different brain regions and by different subsets of neurons. Interpretation of the correlation between resting-state (tonic) α power and intelligence is less clear, but may represent a form of "neural efficiency," by which a high degree of resting α synchronicity reflects low baseline occupation of underlying ensembles, allowing a greater degree of activation (ERD) in response to cognitive load.

Spatiotemporal EEG analysis: Microstate analysis

Traditional techniques of analyzing resting-state EEG, such as those described above, involve analysis of individual waveforms at selected sites of interest over the electrode array, typically converting the recorded signal to the spectral (frequency) domain to make inferences about the nature of patterns of neuronal activity in relation to neurocognitive phenotypes of interest. However, this approach has several important drawbacks. First, it does not encode spatial characteristics of signal simultaneously generated at all electrodes over the scalp, which contains potentially important information about the distribution and temporal dynamics of neural signal generators. Second, conversion to the spectral domain assumes the EEG signal can be represented as a linear dynamical system that can be represented through the Fourier series as a linear function of a set of sine waves. However, neural activity is likely better represented as a nonlinear dynamical system. Furthermore, conversion to the spectral domain requires loss of temporal resolution, which may preclude detection of certain fast neural phenomena. Third, analysis of individual waveforms is highly dependent on the reference electrode(s) selected.

Spatiotemporal analysis is an alternative approach that simultaneously considers the potential recorded at all electrodes over the scalp array, defining a "map topography" of the spatially distributed electric field that is completely independent of the reference chosen. Microstate analysis is one such spatiotemporal approach, in which these instantaneous potential topographies are considered representations of the "state" of the system, and the temporal evolution of these states is analyzed. The method is described in detail in METHODS, and is summarized in FIGURE 1. This method was first proposed by Lehmann in 1987, who showed that the α frequency band (8–12 Hz) of multichannel resting-state EEG could be parsed into discrete states in this way (29). When the multichannel resting-state EEG signal is considered as a time series of topographies of electric potentials, two remarkable properties emerge. First, although there are a large number of possible topographies in multichannel recording, a majority of the signal can be represented by surprisingly few maps. Interestingly, most studies of resting-state EEG consistently find the same four archetypal maps – labeled A, B, C, and D – that explain more than 70% of the total topographic variance. Second, there is a well-defined temporal structure of these maps, in that a single topography remains dominant for about 60-100 ms before abruptly transitioning to another topography. These periods of quasi-stability of a single topography are "microstates." Thus, the multichannel EEG signal can be represented by a single time series of microstates alternating among themselves at discrete intervals.

Compared to traditional frequency power EEG analysis, spatial analysis of EEG using microstates has several advantages. Perhaps most importantly, spatial EEG microstate analysis integrates information from all electrodes over the scalp to generate an instantaneous depiction of the electric field distributed over the entire electrode array. Analysis of the temporal evolution of these electric topographies gives insight into quasi-stable periods of long-range coherence between distant electrodes, reflecting functional coordination within large-scale cortical networks. Furthermore, this technique does not assume the EEG signal is a linear dynamical system. The spatial topography of the EEG signal can be defined at any point in time independently of the preceding or subsequent topography and therefore has sub-millisecond resolution, unlike conventional frequency power analysis that integrates activity over sliding time windows. Finally, microstate maps are completely reference-independent. Microstates are therefore better suited to detect rapid, dynamic activity in large-scale neurocognitive networks than traditional spectral analysis of EEG.

Microstates and resting-state networks

The neurophysiological significance of EEG microstates is not precisely known, but there is evidence to suggest that microstates are each associated with distinct cognitive modalities that arise from the activity of distributed cortical networks. Early indication that EEG microstates encode physiologically relevant information about cortical activity came from several studies observing abnormalities in the microstate time series that were specifically associated with certain neuropsychiatric disorders. For example, the average duration of microstates B and D are significantly shortened in schizophrenia relative to controls (30), while the average duration of microstate C is significantly shortened in frontotemporal dementia (31). Other microstate aberrancies have been noted in Alzheimer's dementia, depression, Tourette's syndrome, and panic disorder, and have been reviewed by the present author elsewhere (32).

In addition to disease states, individual microstates have been associated with specific cognitive modalities. In one early study, volunteers undergoing resting-state EEG recording were asked to write down "what went through his mind just before" an audio prompt was played. The authors found that thoughts related to visual imagery *vs* abstract thought were associated with different preceding microstate topographies (33). A more recent study primed healthy volunteers with visual prompts intended to engage the subject in object-visualization, spatial-visualization, and verbalization cognitive modalities, and found that the percent of total time spent in microstate A was greater during visualization, whereas the percent of total time spent in microstate B was greater during verbalization (34). Taken together, these results indicate that different microstate classes reflect the activity of underlying neural generators that drive distinct modes of cognition.

There is emerging evidence that EEG microstates arise from the activity of so-called resting-state networks (RSNs) that have been identified in functional magnetic resonance imaging (fMRI) studies (35,36). Exploiting the scale-free nature of the EEG microstate time series (37), Britz and colleagues convoluted the EEG microstate time series with resting-state BOLD fMRI signal and found one-to-one temporal correlations between microstates A, B, C, and D, with RSNs associated with phonological processing, the visual network, the saliency network, and attention, respectively (38). Two other studies have also found correlation between microstates and RSNs, but they did not limit their analysis to the four archetypal resting-state EEG microstates found previously and in the study by Britz et al., so a comparison between these findings is difficult (39,40). Nevertheless, these combined EEG-fMRI studies suggest that EEG microstates and fMRI RSNs may arise from the activity of the same underlying neural generators. Although further work is required to corroborate and further explore the association between EEG microstates and RSNs, these preliminary data indicate that microstate analysis may represent a novel approach to interrogating the activity of RSNs at native temporal resolution that is unobtainable by fMRI or other imaging modalities.

Motivation and study design

Our motivation for the present study is as follows. The neurobiological basis of *Gf* remains unclear. Neuroimaging studies have suggested that integrated, distributed parieto-frontal networks play an important role, but the temporal dynamics of these networks are uncertain. EEG microstate analysis is a spatiotemporal approach to multichannel EEG analysis that can give insight into the temporal dynamics of distributed cortical networks. Thus, we endeavor to identify EEG microstate correlates of *Gf* to gain insight into the temporal dynamics of cortical networks that underlie intelligence.

To gain insight into this question beyond a cross-sectional correlational analysis between *Gf* and EEG microstates, some subjects underwent a cognitive training program aimed at transiently increasing *Gf*, as has been successfully accomplished in prior studies. Thus, by examining the degree of convergence between behavioral and microstate patterns observed before and after intervention to improve *Gf*, we hoped to obtain more valuable insight into core neurophysiologic features responsible for fluid cognitive capacity.

In the present study, 64 subjects underwent baseline testing involving resting-state EEG and *Gf* measurement using three standard tasks – Raven's Advanced Progressive Matrices (RAPM), Sandia matrices, and Bochumer Matrizentest (BOMAT). 42 of these subjects underwent 10 cognitive training sessions each lasting 30 minutes on an online platform. After 3 weeks, all subjects were re-tested with resting-state EEG and *Gf* measurement. Microstate analysis was performed on EEG recordings and was correlated with *Gf* measures.

There are multiple models of the role of various brain networks in performing *Gf*-related tasks, each emphasizing different contributions for visual, parietal, and prefrontal regions. Some have argued that increased efficiency at lower levels of processing – early perceptual stages, loaded on occipital and parietal cortices – might enhance higher-level prefrontal computation and therefore represent the primary source of *Gf* variance (41,42). Others suggest that core prefrontal regions related to cognitive control are responsible for the bulk of processing, and play the most relevant role in explaining *Gf* variance (43,44). Intermediate scenarios have also been proposed (45).

These models and the data that underlie them indicate high correlation between visual perceptual regions (early processing), as well as prefrontal regions (cognitive control), and *Gf*. Thus, we hypothesized that (i) features of specific EEG microstates related to the activity of prefrontal and visual areas will display the tightest link with individual *Gf* profiles, with (ii) behavioral changes after cognitive training correlating with modification of the same microstates and little or no involvement of other states. Moreover, we predicted that (iii) successful training outcomes would correspond to an enhancement of the pre-existing relationship between *Gf* and aforementioned microstates.

II. METHODS

Note: Portions of this section have been submitted for publication as:
Santarnecchi E, Khanna AR, Museus C, Benwell C, Davila P, Pascual-Leone A, Shafi MM. EEG microstate correlates of fluid intelligence. Proceedings of the National Academy of Science (Submitted, under review); 2016.

The study protocol described below was approved by the Beth Israel Deaconess Medical Center Ethical committee.

Subject Recruitment

Data were collected as part of an ongoing study at the Berenson Allen Center for Noninvasive Brain Stimulation (Beth Israel Deaconess Medical Center, Boston, MA) designed to test the effect of cognitive training on *Gf*. Participants were recruited from the community by online advertisement, and contacted by e-mail or by phone. Inclusion criteria were as follows: age 18-65 years, normal healthy volunteer, English native-speaker. Exclusion criteria were as follows: corrected visual acuity <60%, pregnancy, sleep deprivation (less than 6 hours a day), history of migraines, history of fainting spells of unknown or undetermined etiology that might constitute seizures, history of seizures, diagnosis of epilepsy, history of abnormal (epileptiform) EEG or family history of treatment resistant epilepsy, contraindication to MRI (e.g. ferromagnetic implant, significant claustrophobia), any implanted medical devices (i.e. Cardiac pacemaker, deep brain stimulator, medication infusion pump, cochlear implant, vagal nerve stimulator) unless otherwise approved by the responsible MD, and substance abuse or dependence within the past 6 months.

Recruitment and selection resulted in a final sample of 74 subjects. These subjects underwent baseline testing, cognitive training or no intervention, and post-training assessment as described below. Six subjects did not complete the cognitive training or post-training assessment, and were excluded from the study. The final sample was composed of 68 subjects (38 males, 30 females), with mean age of 29 years (21-49, SD=12) and a mean of 15 years of education (range 11-23, SD=3).

EEG recording & data preprocessing

Resting-state EEG was recorded using a 20-channel, gel-electrode system from Neuroelectrics (Barcelona, Spain). The system includes 20 leads covering 19 positions of the 10-20 system (C3, C4, O1, O2, Cz, F3, F4, F7, F8, Fz, Fp1, Fp2, P3, P4, Pz, T3, T4, T5, T6) and was recorded at a sampling rate of 500 Hz. Data were collected while the participants sat comfortably with their arms placed on an armrest, eyes open, fixating on a crosshair placed on a white wall in front of them. Recording lasted for 5 minutes.

We used the EEGLAB toolbox (v13.2.1) in MATLAB (vR2012b) to preprocess recorded EEG data (46). Data were first visually inspected, and channels showing significant artifact or noise were removed. Data were filtered for power line noise using a notch filter at 60Hz. The data were bandpassed between 1-100 Hz using a zero-phase second-order Butterworth filter, and were subsequently divided into 3-second epochs. Ocular, muscle, and electrode artifacts were removed using the ADJUST EEGLAB plugin (47), a tool previously developed for independent component analysis (ICA) and semi-automated detection and removal of eye movements and electrode discontinuities. We developed and used custom scripts for removal of independent components corresponding to muscle artifact. Rejected channels were then interpolated using built-in EEGLAB scripts. Cleaned data were used for microstate analysis as described below. Four subjects had EEG recordings with more than 2 channels excluded or with persistent significant muscle or electrode artifact after the ICA preprocessing, and were excluded from the study. Our final sample contained 64 subjects with both pre- and post- training microstate results.

EEG microstate analysis

Microstate analysis of the collected spontaneous EEG recording was performed according to a protocol described and validated elsewhere (48). For each of the 128 individual EEG recordings (64 pre- and post-training), we first identified points of highest topographic signal-to-noise ratio (SNR) by calculating the global field power (GFP) at each data point. The GFP is a single numerical representation of the magnitude of the field strength at each moment in time (49), and is equal to the root-mean-square across the average-referenced electrodes (equivalently, the standard deviation of the signal at all electrodes):

$$GFP(t) = \sqrt{\frac{\sum_{i=1}^{n}[v_i(t) - \bar{v}(t)]^2}{n}}$$

Where $v_i(t)$ is the voltage at electrode i at time t, $\bar{v}(t)$ is the mean voltage across all electrodes at time t, and n is the number of electrodes. Topographies that occur at local maxima of the $GFP(t)$ curve represent instants of highest field strength and greatest SNR. Furthermore, EEG topography tends to remain stable around topographies at local maxima of the $GFP(t)$ curve, and these topographies are representative of topographies at surrounding points in time (48,49). Thus, representation of the original data as a set of topographies at local GFP peaks is a valid method of data reduction. We extracted these topographies at local GFP maxima, hereafter referred to as "original maps" from each of the 128 individual recordings.

Each of the 128 sets of original maps was then individually submitted to a topographic atomize and agglomerative hierarchical clustering (TAAHC) algorithm using the CARTOOL software (50). Details of the TAAHC algorithm can be found elsewhere (48). Briefly, the algorithm begins with each original map considered an independent cluster. Each iteration of the algorithm begins with n clusters, each comprised of a set of member topographies. Each of the n clusters is topographically represented by an "average cluster map," which is derived by taking the electrode-by-electrode mean of the set of member topographies. (In the first iteration, all submitted topographies are considered to be individual clusters.) The "worst" cluster is then identified; in our implementation, this is the cluster with the lowest summated correlation between each constituent map and the average cluster map. Correlation is analogous to the Pearson product-moment correlation coefficient between two vectors:

$$C = \frac{\sum_{i=1}^{n}(u_i \cdot v_i)}{\sqrt{\sum_{i=1}^{n} u_i^2} \times \sqrt{\sum_{i=1}^{n} v_i^2}}$$

The "worst" cluster is eliminated ("atomized"), and its member topographies are reassigned ("agglomerated") to any one of the remaining $n-1$ clusters based on the degree of correlation between the member topography and the average cluster map of each cluster. After each iteration, measures of clustering quality were recalculated. Specifically, we calculated the cross-validation (CV) criteria (51) and the Krzanowski-Lai (K-L) criteria (52). This process is iteratively repeated. After conducting TAAHC on each of the 128 individual recordings, we analyzed the clustering quality metrics for each dataset to identify the optimal number of microstates to identify in the data. Across all 128 individual recordings, CV criteria was minimized at 2.75 ± 0.57 clusters, and the K-L criteria indicated an optimal 4.03 ± 0.39 clusters, suggesting that 3 or 4 clusters would optimally describe the data. This is consistent with a number of prior studies of resting-state EEG that have described optimal clustering with 4 microstate classes (24, 35). Thus, we chose to extract four clusters from each recording.

The data consisted of two subject groups in two conditions (before and after intervention). We collected the four average cluster maps from each EEG recording within each of these four groups and submitted them to another round of TAAHC to derive four group-level representative microstate maps. The four representative microstate maps in each group were labeled A, B, C, and D, and strongly resembled the "archetypal" microstates A, B, C, and D that have been identified in many prior studies (FIGURE 1A) (53). In the final step, the microstates A, B, C, and D from each group were fit onto the original maps from all EEG recordings within each respective group. Each original map is labeled A, B, C, or D depending on which microstate map has the highest correlation to the original map. Thus, each recording can be re-expressed as an alternating sequence of microstates A, B, C, and D. A number of values can be calculated from these sequences. We calculated the average microstate lifespan, frequency of appearance, and fraction total covered time of each microstate – values that have been calculated in numerous prior studies and whose test-retest reliability has been previously validated (48). The lifespan of each microstate is calculated as the time during which all successive original maps were labeled as the same microstate, starting and ending halfway between the last original map of the preceding microstate and the first original map of the following microstate, respectively. The frequency of each microstate is the number of new appearances of each microstate per second. The fraction total covered time of each microstate is the percentage of total time that is spent in each microstate class (note that these three values are not completely independent measures). We compared these values between the two groups and conditions, and determined the correlation between these values and measures of fluid intelligence.

Fluid intelligence measurement

We tested all subjects before and after cognitive training *vs.* no intervention using three different tests previously reported to measure *Gf*, namely, Raven's Advanced Progressive Matrices (RAPM) (54), Sandia matrices (55) and BOMAT (56). As previous authors have argued, these tests of *Gf* likely stress slightly different subcomponents of *Gf*, such as filtering, working memory, visuospatial reasoning, and mental rotation, which in turn load on different brain regions (57,58). Thus, we performed a dimensionality reduction procedure (latent factor analysis) based on principle component analysis (PCA) to use the results of these three tasks to identify independent "factors" encoded in these measures.

RAPM is a commonly used abstract reasoning test considered to be an excellent estimator of *g* (59). The test involves selection of one out of six options given that best completes a rectangular spatial pattern presented in each challenge. RAPM provides a measure of *Gf* by sampling from verbal-analytic and visual-spatial domains that have been shown to be predictive on a variety of related cognitive tasks (59). The number of RAPM stimuli is fixed and limited. In this study, two balanced lists of matrices were created for Pre- and Post-testing by using statistics obtained in a separate longitudinal study of a separate cohort.

Sandia matrices were recently developed as an alternative to RAPM to overcome the fixed number of available Raven's matrices by providing more than 3000 challenges created by combining shape, color, orientation, and other stimuli (55). The structure of Sandia matrices closely resemble RAPM; subjects are presented with a 3x3 stimulus grid with one missing, and given 8 possible choices from which to choose the one that best completes the grid. Each question is categorized based on the number of mental operations required to identify the correct solution; we used only 3-relation matrices in this study to avoid the ceiling effect observed with 1- and 2-relation tests. Furthermore, Sandia questions involve either logical operand manipulation (LOG tasks) or relational syllogisms (REL tasks). In this study, we created two balanced lists of 45 stimuli containing both LOG and REL tasks for testing before and after intervention.

BOMAT was motivated by the need to measure and discriminate *Gf* among high performers. It has similar structure to RAPM and Sandia; the subject is asked to identify the missing item that best completes a pattern of a 5x3 matrix, choosing from six options. In this study, we used the "advanced-short" version of BOMAT. Two lists of stimuli were been created as specified in the test manual for pre- and post-testing.

Identification of task-independent components of fluid intelligence

To obtain task-independent measures of *Gf*, and to attempt separation among components of *Gf* that load on different cognitive substructures, we performed a PCA procedure on these three *Gf* measures (RAPM, Sandia, and BOMAT) to identify independent components measured by these tests. This PCA procedure is based on the varimax rotation (60) applied on the correlation matrix of the results obtained from each measure. Given prior evidence that Sandia LOG and REL components engage different cognitive processes that load on different brain regions, these were considered as separate measures (55). At baseline (pre-intervention), scores on *Gf* tests were (mean +/- SD, range): RAPM, 77% +/- 15%, 13-100%; Sandia-LOG, 57% +/- 16%, 19-94%; Sandia-REL, 57% +/- 16%, 18-82%; and BOMAT, 54% +/- 23%, 7-100%. We employed a data-driven approach to select the optimal number of components among these scores (eigenvalue > 1), which resulted in two components (FIGURE 2A; component 1 eigenvalue = 3.355, component 2 eigenvalue = 1.24, total variance explained = 81%, component 1 variance explained = 58%, component 2 variance explained = 23%). Component 1 (*Gf-1*) includes scores from RAPM and Sandia-LOG, whereas component 2 (*Gf-2*) includes scores from BOMAT and Sandia-REL. We applied the Bartlett transformation on individual scores to convert scores on the administered tests into weighted component values. The Bartlett transformation is a least-squares procedure which minimizes the sums of squares of the factors over the range of variables, and is advantageous for its univocality, i.e. each variable is highly correlated with one factor only, enabling easier interpretation (61). The transformed scores (*Gf-1* and *Gf-2*) did not show any sex differences (FIGURE 2D).

Cognitive training

42 subjects underwent a computer-based executive-function training program developed for this study by SIM-COACH Games (http://www.simcoachgames.com/). This computer game is based on multiple executive function tasks, including working memory, inhibitory, and switching abilities (62,63), and includes an adaptive progression algorithm that allows the user to move to higher levels only after specific proficiency is achieved. At higher levels, users are also challenged with logical operands (e.g. AND, OR, XOR) for training of abstract-reasoning skills.

Training involved 10 sessions each lasting 30 minutes over the course of two weeks that was administered under observation at our laboratory. Participants received brief instructions prior to the first training session, and then received hints and suggestions as needed during the course of training. 26 subjects did not receive any intervention for 3 weeks, only receiving pre- and post-*Gf* and EEG measurements.

A few prior studies have indicated that transcranial electrical stimulation may be effective in improving *Gf* or potentiating its improvement by interventions designed to improve *Gf*, such as cognitive training (64,65). In an effort to achieve this effect, some participants underwent transcranial electric stimulation concurrently during the training program (transcranial random noise stimulation, n=13; transcranial direct current stimulation, n=10; multifocal transcranial direct current stimulation, n=8; transcranial alternating current stimulation, n=7). The objective of the present study was not to examine or delineate among the effects of transcranial stimulation; thus, they are not considered in the following analysis. However, they were included in the final statistical model as covariates.

Statistical analysis

All analyses were performed using IBM SPSS Statistics (Version 21, release 21.0.0) and MATLAB (Release 2012b, Mathworks).

Baseline correlates of *Gf*

To determine baseline correlates of *Gf*, the Pearson product-moment coefficient between both *Gf* Bartlett scores and factors calculated from the microstate time series (frequency, coverage, average life, GFP peaks/appearance, transition probabilities among microstates, global GFP peaks/sec, global frequency, and global average life) were calculated. The results are displayed for all n=64 subjects prior to intervention, with $\alpha=0.05$ corrected for multiple comparisons using the Bonferroni correction.

Changes in *Gf* and microstate properties after cognitive training

Separate repeated measures Analysis of Covariance (rm-ANCOVA) models for *Gf-1*, *Gf-2,* and all microstate time series properties (listed above) were constructed, including factors “TIME” (2 levels, PRE vs POST) and “INTERVENTION” (2 levels, TRAINING *vs.* CONTROL). Gender, age, education, and transcranial electric stimulation group were included as covariates. In the event of significant TIME or INTERVENTION effects, further simple main effects were analyzed using a similarly structured ANCOVA to decompose the effect. Post-hoc comparisons were conducted using $\alpha=0.05$ corrected using the Bonferroni correction for multiple comparisons.

Microstate topographic changes after cognitive training

The impact of cognitive training on microstate structures was evaluated with a topographic analysis of variance (TANOVA) test to compare each microstate class (A, B, C, and D) among the two subject groups in the two conditions (TRAINING *vs.* CONTROL). TANOVA utilizes randomization statistics to test the magnitude of the difference between two groups of maps against the null hypothesis that the assignment of maps to groups is random (66). The two groups of maps to be compared are each electrode-by-electrode averaged to produce two group-averaged maps. The test statistic representing the magnitude of the difference between these two group-averaged maps is the global map dissimilarity between them:

$$GMD(u,v) = \sqrt{\frac{\sum_{i=1}^{n}(u_i - v_i)^2}{n}}$$

Where u_i and v_i are the potentials at electrode i in the maps being compared.

After the actual test statistic is calculated, the maps are randomly shuffled between the two groups, and the test statistic is recalculated. This process is repeated 5000 times to generate a distribution of test statistics under the null hypothesis that the maps are randomly distributed between the two groups. The fraction of test statistics greater than the actual test statistic is the *p*-value.

Interaction between microstate changes and *Gf* changes after cognitive training

Changes in *Gf-1* and *Gf-2* after cognitive training (*vs.* no contact) were calculated for the entire sample, and correlated with all calculated microstate properties (frequency, coverage, average life, GFP peaks/appearance, transition probabilities, global GFP peaks/sec, global frequency, and global average life). Changes were calculated in a paired fashion: baseline scores were subtracted from post-intervention scores to obtain the magnitude and direction of change in each measure. Post-intervention *Gf* scores were subjected to the Bartlett transformation based on weights obtained on pre-intervention data. All analyses were conducted with α=0.05 corrected for multiple comparisons with the Bonferroni correction.

III. RESULTS

Note: Portions of this section have been submitted for publication as:
Santarnecchi E, Khanna AR, Museus C, Benwell C, Davila P, Pascual-Leone A, Shafi MM. EEG microstate correlates of fluid intelligence. Proceedings of the National Academy of Science (Submitted, under review); 2016.

Baseline correlates of Gf

All microstate values calculated are reported in SUPPLEMENTARY TABLE 1. Correlation between *Gf* scores and microstate values revealed distinct patterns of correlation between specific microstate values and *Gf-1 vs. Gf-2*. There was a significant negative correlation between *Gf-1* and the frequency of microstate C ($r = -0.503$, $p = 0.002$) and the average number of GFP peaks/sec ($r = -0.451$, $p = 0.008$). There was a significant negative correlation between *Gf-2* and the frequency of microstate B ($r = -0.346$, $p = 0.012$), the transition probability of A→B ($r = -0.281$, $p = 0.019$), and the transition probability of D→B ($r = -0.279$, $p = 0.018$). A full set of correlation coefficients is presented in SUPPLEMENTARY TABLE 2.

Changes in Gf *after cognitive training*

The rm-ANCOVA model for Gf-2 revealed significant effects of TIME [$F(1,132) = 4.376$, $p<0.05$] and INTERVENTION [$F(1,132) = 4.931$, $p<0.01$], with a significant interaction between the two factors [$F(1,132) = 4.74$, $p=0.023$]. The simple main effect for TIME was significant for *Gf-1* [$F(1,132) = 9.79$, $p<0.01$; +16%] and *Gf-2* [$F(1,132) = 7.43$ $p=0.009$; +28%] (FIGURE 4A). The simple main effect for INTERVENTION was significant only for *Gf-2* [$F(1,132) = 4.73$, $p=0.019$]. The significant interaction term was driven by an improvement in *Gf-2* scores observed in the cognitive training group, but not for participants in the no-contact group [$t(61) = 3.92$, $p=0.012$].

Topographic changes in microstates after cognitive training

Individual microstate topographies are thought to emerge from the activity of underlying brain networks. To identify whether cognitive training affects microstate topographies, we extracted a set of four microstates from each subject before and after intervention. These topographies were each labeled A, B, C, and D depending on the degree of correlation between each map and the “archetypal” maps A, B, C, and D that have been identified in many previous studies (24, 35, 88). The set of maps A, B, C, and D were compared across conditions using TANOVA as described in Materials and Methods. There were no significant differences between the topographies of A, B, C, or D between controls and subjects at baseline ($p>0.05$ for each comparison between maps A, B, C, and D). Controls did not show any significant difference in topographies 3 weeks after baseline evaluation. However, among subjects who underwent cognitive training, there was a significant difference in microstate C following intervention ($p=0.0064$). Topographically, this corresponded to a more posterior isoelectric point in the map of microstate C after cognitive training (FIGURE 4B). No other significant differences among groups were found.

Changes in microstate properties after cognitive training

The rm-ANCOVA revealed significant effects of TIME [$F(1,132) = 8.749$, $p<0.01$] and INTERVENTION [$F(1,132) = 7.575$, $p<0.01$], whereas a significant interaction between the two factors was not present [$F(1,132) = 0.43$, $p=0.253$]. Simple main effects of TIME and INTERVENTION were analyzed separately. The simple main effect for TIME was significant for average life of microstate C [$F(1,132) = 10.92$, $p<0.006$; +8.2%] and microstate D [$F(1,132) = 7.91$, $p<0.002$; –9.8%] (see Figure 5A-B), with similar changes for the frequency and coverage of microstates C and D, respectively, but that were not statistically significant.

Correlation between changes in microstates and changes in Gf *scores*

Differences in *Gf-1* and *Gf-2* obtained at before and after intervention were calculated and correlated with changes in microstate properties (frequency, coverage, GFP peaks, transition) for microstates A, B, C and D, for both cognitive training and no contact (control) groups. We found a significant negative correlation between the fraction coverage of microstate B and changes in *Gf-2* for participants undergoing the cognitive training ($r = –0.379$, $p = 0.012$) (FIGURE 5C), but not among control subjects.

IV. DISCUSSION, CONCLUSIONS, & SUGGESTIONS FOR FUTURE WORK

Note: Portions of this section have been submitted for publication as:
Santarnecchi E, Khanna AR, Museus C, Benwell C, Davila P, Pascual-Leone A, Shafi MM. EEG microstate correlates of fluid intelligence. Proceedings of the National Academy of Science (Submitted, under review); 2016.

Human intelligence has been related to several intrinsic properties of the human brain interrogated using a variety of neuroimaging and electrophysiological techniques. An emerging consensus derived from studies using these techniques emphasizes the role of distributed brain regions functionally organized into large-scale networks that facilitate progressively higher orders of cognitive processing that collectively constitute intellectual ability (22,67). Scalp EEG is capable of depicting the brain's electrical activity at native timescales, and the use of spatiotemporal microstate analysis of multichannel EEG may give insight into the activity of large-scale cortical networks at unprecedented temporal resolution. Previous studies of EEG microstate analysis have correlated each microstate class with distinct cognitive functions (34) and activation of distinct brain regions (38). Based on these prior data, we hypothesized that *Gf* would most closely relate to microstate features associated with visual networks (reflecting low-level visual/perceptual processing loaded on occipital and parietal regions) as well as microstate features associated with prefrontal activation (reflecting higher-level cognitive processing). Furthermore, we hypothesized that improvement in *Gf* after cognitive training would be reflected by changes in microstate features specifically limited to these networks.

Overall, our data confirm our hypotheses by showing that *Gf* is inversely correlated with specific properties of microstates B and C, which have previously been shown to load on prefrontal and occipital regions, respectively (38). A shift in topography of state C was observed after cognitive training aimed at increasing fluid intelligence. Separation of *Gf* into two independent components revealed that components *Gf-1* and *Gf-2* were specifically correlated with microstate C and B, respectively, suggesting that these microstates represent distinct cognitive processes. Finally, improvement in *Gf-2* after cognitive training was significantly correlated with reduction in the stability (average lifespan) of microstate B. The present results suggest a pivotal role for brain regions related to visual processing and executive control networks in *Gf*. These data are also a compelling demonstration of how intervention to raise *Gf* can be a powerful method to identify neurophysiological correlates of *Gf*. Furthermore, these findings indicate that EEG microstate analysis is a powerful method to interrogate cortical network electrophysiology with high temporal resolution, and can supplement other methods, such as fMRI, to provide additional insight into the function and significance of cortical networks.

Gf components and activity in visual and cognitive control regions

Measurement of *Gf* with any single standardized assessment is complicated by the multidimensional nature of *Gf* and the likely involvement of multiple different cognitive processes, including working memory, pattern recognition, mental rotation, filtering, inhibition of irrelevant stimuli, and others (68–70). We measured *Gf* in our sample using three well-studied tests (RAPM, Sandia, and BOMAT), which engage slightly different, but overlapping cognitive processes. To derive two independent measures of *Gf* from scores on these tests, we applied latent factor analysis and successfully delineated among two distinct factors – *Gf-1* and *Gf-2* – that were mathematically independent and comprised of distinct sets of scores; *Gf-1* is comprised of RAPM and Sandia-LOG, while *Gf-2* is comprised of Sandia-REL and BOMAT. The distinction among these tests may be due to the nature of the stimuli presented in each, which is further reflected by the fact that *Gf-1* and *Gf-2* correlated with different EEG microstate classes.

Gf-1 is driven by RAPM and Sandia-LOG scores, and is (inversely) associated with the frequency of microstate C. A seminal prior study by Britz and colleagues determined that microstate C is most closely associated with the so-called "salience network," a resting-state functional network between the anterior cingulate cortex (ACC), bilateral inferior frontal gyri, right anterior insula, and left claustrum (38). Together, these regions are known to be crucial nodes for executive function and processing of logical or conditional rules, which have been repeatedly shown to correlate with performance in RAPM and similar abstract reasoning tasks (71,72). Furthermore, one functional study suggested that gray matter volume and homogeneity of regions belonging to the salience network are significantly associated with *Gf* measured by RAPM (73). Together, these prior studies seem consistent with ours in suggesting that the correlation between *Gf-1* and microstate C is a result of activation of cortical and subcortical regions comprising the salience network as defined my numerous prior functional studies.

The second component, *Gf-2*, loads on BOMAT and Sandia-REL scores, and is (inversely) associated with the frequency of microstate B. Britz and colleagues have previously associated microstate B with BOLD activity in the bilateral extrastriate visual areas (Brodmann Areas 18 and 19), which are known to be involved in spatial attention (74–76). This suggests that performance on BOMAT and Sandia-REL, together comprising *Gf-2*, relate to the spontaneous activity of the parieto-occipital cortex, possibly reflecting cognitive processes such as visual search, feature selection, and visuospatial abilities, as compared to prefrontal abstract reasoning skills. Notably, BOMAT matrices present a more dense array of stimuli than Sandia (5x3 *vs* 3x3 grid into which subjects must fill in the missing piece); this may elicit larger involvement of visual areas during the early stages of visual problem solving and demand a higher visual working memory load (77). Based on this reasoning, some have suggested that BOMAT (and perhaps Sandia-REL) engages subcomponents of *Gf* related to visual processing and visual working memory, rather than purely abstract reasoning (prefrontal) processes (57). This seems consistent with the statistical delineation between *Gf-1* and *Gf-2* based on the scores we obtained in our study. Based on the tests and microstates with which they are most associated, *Gf-1* appears to reflect a cognitive control, prefrontal network, while *Gf-2* appears to reflect a visual cortical network related to visuospatial working memory.

Higher fluid intelligence, reduced specific microstate activations

The observed negative correlation between specific microstates properties and Gf offers an interesting insight about the relationship between microstates and spontaneous cerebral activity patterns. Specifically, if the frequency of appearance of a microstate class represents the propensity for its underlying neural generators to become activated (32), our results suggest that increasing *Gf-1* and *Gf-2* scores correlate with relatively reduced resting-state engagement of the networks underlying microstate C and B, respectively. There are two possible explanations for these inverse associations. First, this may represent a form of so-called "neural efficiency," whereby lower activity of the network in the resting state represents heightened efficiency and enables better performance during a cognitive task (78,79). In our subjects, lower spontaneous recruitment of microstate B or C at rest may represent more "reserve" to be exploited during relevant cognitive engagement. Alternatively, these individuals may have lower activation of networks underlying microstate B or C in general, due to greater network efficiency regardless of cognitive demand (80,81).

A second potential explanation for the negative association between *Gf* scores and the frequency of microstates B and C was recently proposed by Milz et al., who remarked that oscillations within the alpha band, which dominates the frequency bandwidth from which microstates are calculated, typically represents inhibitory rather than excitatory control on modality-specific processing (34). The authors postulate that decreasing microstate activity may actually reflect disinhibition of the underlying brain regions and corresponding cognitive processes (34). Under this hypothesis, the α synchronization reflected by the appearance of a microstate represents an "idle state" of its underlying network(s), and activity of these underlying network(s) is associated with α desynchronization – analogous to the ERD effect that has been reported previously in EEG intelligence literature. Alternatively, they suggest that if decreasing activity of a given microstate class reflects reduced activity of corresponding brain regions, that this reduced activity might represent release of tonic inhibition on other brain regions or processes. According to this reasoning, our finding of decreasing frequency of microstate C correlating with increasing *Gf-1* may reflect reduced inhibition of frontal control networks (e.g. ACC, inferior/middle frontal gyri), or may reflect reduced inhibition by frontal control networks on other networks. Similarly, decreasing activation of microstate B, which shows a right-posterior source in the study by Milz and colleagues (i.e. parieto-occipital), may be associated with disinhibition of areas related to visuospatial processing – such as the right posterior parietal cortex (82) – correlating with increasing *Gf-2* scores.

Moreover, Milz and colleagues also related individual microstate classes with particular modalities of thinking, specifically "object visualization," "spatial visualization," and "verbalization", compared to rest (34). Interestingly, the authors report that both object and spatial visualization were associated with increased average lifespan (here, interpreted to reflect increased stability of underlying networks) of microstate C, related to sources in prefrontal regions that are putatively less relevant for object/spatial visualization. On the other hand, the frequency, duration, and coverage of microstate B was increased in verbalization compared to visualization (i.e. increased inhibition of non-verbal, posterior regions). This is consistent with our findings relying on a *Gf* assessment based on culture-fair tasks (83,84), inherently loading more on object and spatial visualization than verbalization.

Clearly, such precise association between specific microstates and behavior requires much additional validation, and should be interpreted carefully. Regardless of a putative role assigned to a given microstate, any behavioral or mental modality implies the co-existence of all microstates classes identified so far (34). Thus, the ratio of relative contributions of microstates is likely more relevant to ongoing resting-state brain activity than the absolute dominance of a single microstate during any given moment.

Intelligence, the α rhythm, and microstates

A number of studies employing spectral EEG analysis have described a complex relationship between α power and cognitive performance (23,24,85,86). When EEG is recorded in the resting state, α power positively correlates with performance in a number of cognitive tasks, including semantic memory performance, verbal reasoning and tests of general intelligence such as the IST-70 and LGT-3 (24). We have recently shown that α power is strongly negatively associated with overall microstate frequency (48). Furthermore, given that the GFP curve is driven by the dominant frequency band in the EEG signal, the number of GFP peaks per second is positively correlated with increasing α power and negatively correlated with increasing β power (Khanna et al., unpublished results). Our parsing of the EEG signal into discrete microstates enabled us to identify changes within individual microstate classes that underlie the negative correlation between GFP peaks/sec and *Gf-1* in our data. Indeed, reduced GFP peaks/sec in the overall data did not translate to a reduced frequency of all microstates, as might be expected in the case of a global oscillation slowing (or a global increase in relative α power); instead, this effect was limited to a reduced frequency of one specific microstate class, i.e. microstate C. Together, these data suggest that a slowing of the activity of the neural generators underlying microstate C relates to intelligence, an idea corroborated by the corresponding significant change in microstate C topography observed after cognitive training. These results also show that EEG microstate analysis can identify changes in the spatiotemporal dynamics of specific neural generators otherwise undetectable using traditional spectral EEG analysis.

Enhanced cognition, decreased inhibition?

Participants who underwent a cognitive training program aimed at improving fluid intelligence had a significant increase in *Gf-2* scores; no such improvement was seen in control subjects who did not undergo cognitive training. The cognitive training group also showed a change in the topographic map corresponding to microstate C, characterized by a posterior shift in the isoelectric point. In addition, the degree of *Gf-2* improvement after training was significantly negatively correlated with the change in the stability (average lifespan) of microstate B (FIGURE 5B). The negative correlation between changes in stability (average lifespan) of microstate B and *Gf-2* scores after training is consistent with the context highlighted by Milz and colleagues as discussed above (34), and supports the association between microstate B and cognitive modalities related to *Gf-2* that were identified at baseline in our dataset. Specifically, as discussed above, better baseline *Gf-2* scores, which negatively correlated with the frequency of microstate B, could be related to resting-state disinhibition of posterior visual processing regions. Therefore, the negative correlation between changes in microstate B lifespan and the improvement in *Gf-2* scores suggests that a training-associated disinhibition of visual regions – captured by microstate B activity – is associated with (and in fact may underlie) improvement on the BOMAT and Sandia-REL *Gf* tasks (in our data, *Gf-2*). However, whether the changes in microstate B activity are causally related to the improvement in task performance cannot be assessed using our data.

The interpretation of changes in the topography of microstate C is more complex. We suggest that our finding of a more posterior centroid for microstate C after cognitive training might reflect integration of more posterior regions with the frontal executive/control networks, typically thought to be involved in microstate C activity (38,87). Interestingly, prior studies assessing the impact of various forms of cognitive training (e.g. inhibition, task switching) have shown a shift in the pattern of fMRI activations after training, describing an increased prefrontal activation with corresponding reduction in contribution from parietal regions (88). This dynamical rearrangement of cognitive resources, pointing to a switch from the "perceptual to the logical brain" (88) might fit with the posterior displacement observed in our data, as a reflection of an increased frontally-mediated inhibitory control towards posterior regions (89,90). Other studies have supported such a hypothesis by showing that regions involved in inhibitory control (e.g. dorsolateral, inferior and medial prefrontal cortices) are more engaged when participants successfully overcome perceptual mismatches – a process engaging the parietal lobes – in order to provide a logical response (91).

Overall, the present data suggest a training-related (i) increase of prefrontal cognitive control of parietal regions, and a (ii) disinhibition of visual areas specifically associated with a *Gf* component requiring visuospatial processing, as potential correlates of fluid intelligence improvement in humans. Further studies, possibly including multiple imaging techniques (e.g. fMRI and perfusion MRI), are warranted to verify such hypotheses and to test for the additional crucial role played by top-down modulation processes involving prefrontal and visual areas suggested by our data (44). The present findings also highlight the value of addressing the quest for the neurobiological basis of human intelligence by means of a confirmatory approaches based on "cognitive perturbation" aimed at observing convergence of behavioral and neurophysiological results, which extend beyond the speculative nature of correlational studies.

Limitations

There are a number of limitations to this study that warrant careful consideration. The motivation of this study was to identify neurophysiological correlates of human fluid intelligence. To achieve this goal, we used a spatiotemporal EEG analytic method designed to detect the activity of large-scale cortical networks to identify correlates of *Gf* in a cohort of healthy volunteers, and implemented a 3-week cognitive training program to examine the convergence between *Gf* improvement and microstate correlates.

We were successful in identifying baseline microstate correlates of two mathematically independent factors of *Gf*, and attempted to interpret these correlations based on previous data examining the relationship between microstates, cognitive modes, and RSNs. However, the relationship between the four resting-state microstates we identified in our data and RSNs has only been explored in a single study (38), and although other studies relating microstates with RSNs have been published (40), these studies did not use a consistent set of microstate topographies and had significant methodological differences, so comparison among them is difficult. Although there are converging lines of evidence to suggest that microstates and RSNs arise from the same set of signal generators (32,38,40,92), the specific assignment of brain regions or networks to RSNs and microstates requires additional validation. Furthermore, although fMRI has been able to identify functionally correlated brain regions in the resting state, these measurements require time averaging over about 5 minutes, and so are incapable of discerning whether all identified regions within the network are simultaneously active, or synchronized at specific phase delays – indeed, anatomic identification of RSNs using fMRI does not give any temporal information about the nature of their functional correlation. Thus, although Britz and colleagues identified temporal correlation between the microstate time series and the BOLD signal, without information about which component(s) of each RSN are active at any given epoch of the BOLD signal, correlation with microstate topographies is difficult, and one-to-one assignments between RSNs and microstates should be interpreted with caution.

We attempted to supplement a cross-sectional correlation between *Gf* and EEG microstates by employing a cognitive training program aimed at increasing *Gf* based on published data suggesting that such transient improvement in *Gf* is possible using a cognitive training program (14,15). However, these data have been criticized on methodological grounds, as well as on the broader question of how intelligence is quantified and how changes in intelligence quantification can or should be interpreted (93). In our study, subjects improved in *Gf-2* but not *Gf-1*, suggesting improvement in visuo-spatial processes but not executive, prefrontal tasks. The significance of this finding is uncertain. It may reflect genuine improvements in task-independent visuo-spatial reasoning ability, or may reflect task-specific improvements that are a result of repeated exposure to related stimuli during training. Furthermore, the real-world importance of such improvements in visuo-spatial reasoning, and their application to problems other than the tests we employed, remain to be seen.

Finally, we are limited by the cognitive training design in failing to achieve significant improvements in *Gf-1* in order to supplement baseline microstate correlations. It is unclear whether an alternative cognitive training program may have been able to induce improvements in *Gf-1* to achieve this aim; future studies are warranted to determine this possibility.

Further studies

The results and limitations of this study suggest promise for future investigation. These future studies should focus on two broad topics: first, improvement of the method of EEG microstate analysis, and second, further study into the neurophysiological processes that together generate *Gf*.

The method of EEG microstate analysis has undergone considerable evolution since it was first proposed in 1971. The current approach involves two primary steps: first, microstate maps are identified using a mathematical clustering algorithm applied to original maps in the data; and second, the original maps are each assigned to the microstate with which it best correlates, enabling re-expression of the series of original maps as a sequence of alternating microstates. Although this approach yields reliable results (48), future studies should explore optimization of each step in this approach.

First, the use of mathematical clustering algorithms (e.g. *k*-means clustering, or atomize and agglomerative hierarchical clustering) to identify natural clusters within the data suffers the same set of challenges inevitable in mathematical clustering procedures in general. Perhaps most importantly, clustering gives no information about how many clusters naturally occur within the data or "optimally" describe the data. In resting-state EEG microstate analysis, this manifests as uncertainty about the "correct" number of microstates to extract from the pool of original maps. Because of the number of degrees of freedom in even 19-channel EEG, and given an expected level of noise in the signal, more microstate maps will always explain a greater proportion of total variance. To address this ambiguity, mathematical criteria have been proposed to evaluate the "correctness" of each number of clusters (51,52), but these encode implicitly subjective weights to certain factors, and may not be valid for all electrode montages (94). Finally, these clustering algorithms are frequently computationally intensive. An alternative to traditional mathematical clustering analysis to identify microstate maps should be considered in future studies. This may come from the field of nonlinear dynamical analysis (95). Specifically, each instant of the multichannel EEG signal (represented by a topographic map) can be expressed as a vector with dimension equal to n electrodes; this vector can be embedded into phase space with dimension n, from which features of the evolution of the complex multidimensional time series may be calculated. In fact, in its current implementation, the process of microstate analysis can be thought of as a procedure involving spatial embedding of the signal into phase space and re-representation of the nonlinear time series using symbolic dynamics, where the phase space is partitioned according to proximity to each microstate map (96). The use of tools in nonlinear dynamical analysis to extract the microstates themselves is less clear, but nevertheless promising. For example, a method to generate data-driven partitions of phase space for use in symbolic dynamic analysis has been proposed, which may be able to extract nodes representing microstate maps (97). We speculate that, in phase space, microstates would manifest as unstable periodic orbits (UPOs) around attractors of the nonlinear system (98–100); techniques to extract these UPOs and attractors have been proposed (100–103), and may be useful in identifying microstates (attractors) without traditional clustering methods.

In the second step of microstate analysis, original maps are each assigned a label based on which microstate map it most resembles. In general, original maps have high correlation with one of the microstate maps, and the assignment is a valid method of data re-expression. However, there are original maps that do not resemble any of the microstate maps – yet the algorithm as currently implemented forces an assignment to one of the microstate maps and thereby detracts from the validity of data re-expression as a series of microstate maps. The original maps that do not resemble any microstate could represent a microstate not represented by the applied set of microstate maps, may reflect brief periods of chaos within the otherwise periodic signal evolution centered about microstate attractors (104), or could be a product of noise or artifact. Delineating among these possibilities will be laborious, but immediate improvement in the validity of data re-expression can be achieved by assigning an original map to a microstate only if the correlation between them meets a certain threshold. In this way, ambiguous original maps do not distort the microstate model. We are currently investigating this improvement. Overall, rethinking microstate analysis as an implementation of nonlinear dynamical analysis may yield novel approaches to these and other methodological questions.

The current results also point to exciting new areas of investigation into the neural basis of *Gf*. For example, adding additional functional imaging modalities to this experimental paradigm, such as fMRI or PET, would enlighten the interpretation of microstate correlations with *Gf*. Our study indicates that different microstates correlate with distinct factors of *Gf*; this can be corroborated and further explored by using tests of intelligence other than the three used here that are known to engage different cognitive processes. Additionally, further studies evaluating microstate syntax during various steps of the abstract-reasoning processes (e.g. during rule inference *vs.* response generation phases) (77) could confirm and expand on current findings. Finally, our results suggest that neurophysiological monitoring using EEG microstates are effective in detecting changes in the brain that correspond to improvements in performance on tests designed to measure *Gf*; therefore, EEG microstates may be valuable in future studies examining the effect of cognitive training, transcranial electric stimulation, or other interventions designed to improve *Gf*.

V. SUMMARY

In this study, we sought to use EEG microstate analysis to study neurophysiological correlates of fluid intelligence (*Gf*) in healthy humans by examining microstate correlates of *Gf* at baseline and after a 3-week cognitive training program designed to improve *Gf*. We show that *Gf* scores measured by three common tests are differentiable into two factors. These factors correlate with microstates associated with cognitive control (microstate C) and visuospatial processing (microstate B), respectively. Cognitive training significantly improved scores in the *Gf* factor related to visuospatial processing, which was accompanied by destabilization of the corresponding microstate (B). Cognitive training also caused a significant posterior shift in the topography of microstate C, possibly reflecting greater integration of parietal circuits in frontal cognitive control processes. The degree of spontaneous activity of brain regions related to cognitive control and visual processing seems able to explain both variability in individual cognitive profile and the response to a cognitive training exerting significant changes on fluid intelligence levels. The present data also support the idea that EEG microstates represent an "idle state" of underlying cognitive networks, offering a new insight about the link between human fluid intelligence and spontaneous EEG activity. Furthermore, our findings confirm that EEG microstate analysis is a powerful method to interrogate cortical network electrophysiology with high temporal resolution to provide insight into the function and significance of cortical networks related to *Gf*.

VI. REFERENCES

1. Spearman C. "General Intelligence," Objectively Determined and Measured. Am J Psychol [Internet]. University of Illinois Press; 1904;15(2):201–92. Available from: http://www.jstor.org/stable/1412107
2. Salthouse TA. Localizing age-related individual differences in a hierarchical structure. Intelligence. 2004 Nov;32(6).
3. Deary IJ, Penke L, Johnson W. The neuroscience of human intelligence differences. Nat Rev Neurosci. England; 2010 Mar;11(3):201–11.
4. Deary IJ. Looking Down on Human Intelligence: From Psychometrics to the Brain [Internet]. Oxford University Press; 2000. Available from: https://books.google.com/books?id=GJcQAQAAIAAJ
5. Cattell RB. Intelligence: Its Structure, Growth and Action [Internet]. Elsevier Science; 1987. Available from: https://books.google.com/books?id=flX770mG2HcC
6. Carroll JB. Human Cognitive Abilities: A Survey of Factor-Analytic Studies [Internet]. Cambridge University Press; 1993. Available from: https://books.google.com/books?id=jp9dt4_0_cIC
7. Ackerman PL, Beier ME, Boyle MO. Working memory and intelligence: the same or different constructs? Psychol Bull. United States; 2005 Jan;131(1):30–60.
8. Hunt E. Let's hear it for crystallized intelligence. Learn Individ Differ [Internet]. 2000 Mar;12(1):123–9. Available from: http://www.sciencedirect.com/science/article/pii/S1041608000000339
9. Cattell RB. Abilities: Their Structure, Growth, and Action [Internet]. Houghton Mifflin; 1971. Available from: https://books.google.com/books?id=9dRq2P9SI5QC
10. Moffitt TE, Caspi A, Harkness AR, Silva PA. The natural history of change in intellectual performance: who changes? How much? Is it meaningful? J Child Psychol Psychiatry. ENGLAND; 1993 May;34(4):455–506.
11. Deary IJ, Whalley LJ, Lemmon H, Crawford JR, Starr JM. The Stability of Individual Differences in Mental Ability from Childhood to Old Age: Follow-up of the 1932 Scottish Mental Survey. Intelligence [Internet]. 2000 Feb;28(1):49–55. Available from: http://www.sciencedirect.com/science/article/pii/S0160289699000318
12. CATTELL RB. THE HERITABILITY OF FLUID, gf, AND CRYSTALLISED, gc, INTELLIGENCE, ESTIMATED BY A LEAST SQUARES USE OF THE MAVA METHOD. Br J Educ Psychol [Internet]. Blackwell Publishing Ltd; 1980 Nov 1;50(3):253–65. Available from: http://dx.doi.org/10.1111/j.2044-8279.1980.tb00809.x
13. Davies G, Tenesa A, Payton A, Yang J, Harris SE, Liewald D, et al. Genome-wide association studies establish that human intelligence is highly heritable and polygenic. Mol Psychiatry. Nature Publishing Group; 2011;16(10):996–1005.
14. Jaeggi SM, Buschkuehl M, Jonides J, Perrig WJ. Improving fluid intelligence with training on working memory. Proc Natl Acad Sci U S A. 2008;105(19):6829–33.
15. Au J, Sheehan E, Tsai N, Duncan GJ, Buschkuehl M, Jaeggi SM. Improving fluid intelligence with training on working memory: a meta-analysis. Psychon Bull Rev [Internet]. 2015;22(2):366–77. Available from: http://link.springer.com/10.3758/s13423-014-0699-x
16. Santarnecchi E, Polizzotto NR, Godone M, Giovannelli F, Feurra M, Matzen L, et al. Frequency-Dependent Enhancement of Fluid Intelligence Induced by Transcranial

Oscillatory Potentials. Curr Biol [Internet]. Elsevier Ltd; 2013;23(15):1449–53. Available from: http://linkinghub.elsevier.com/retrieve/pii/S0960982213007136
17. Santarnecchi E, Muller T, Rossi S, Sarkar A, Polizzotto NR, Rossi A, et al. Individual differences and specificity of prefrontal gamma frequency-tACS on fluid intelligence capabilities. Cortex. 2015 Nov;75:33–43.
18. Pahor A, Jaušovec N. The effects of theta transcranial alternating current stimulation (tACS) on fluid intelligence. Int J Psychophysiol [Internet]. 2014;93(3):322–31. Available from: http://www.ncbi.nlm.nih.gov/pubmed/24998643
19. Deary I. Why do intelligent people live longer? Nature [Internet]. Nature Publishing Group; 2008 Nov 13;456(7219):175–6. Available from: http://dx.doi.org/10.1038/456175a
20. Batty GD, Deary IJ, Gottfredson LS. Premorbid (early life) IQ and Later Mortality Risk: Systematic Review. Ann Epidemiol. 2007;17(4):278–88.
21. Whalley LJ, Deary IJ, Appleton CL, Starr JM. Cognitive reserve and the neurobiology of cognitive aging. Ageing Res Rev. England; 2004 Nov;3(4):369–82.
22. Jung RE, Haier RJ. The Parieto-Frontal Integration Theory (P-FIT) of intelligence: converging neuroimaging evidence. Behav Brain Sci. 2007;30(2):135–54; discussion 154–87.
23. Klimesch W. EEG alpha and theta oscillations reflect cognitive and memory performance: a review and analysis. Brain Res Rev [Internet]. 1999;29(2-3):169–95. Available from: http://www.sciencedirect.com/science/article/pii/S0165017398000563
24. Doppelmayr M, Klimesch W, Stadler W, Pöllhuber D, Heine C. EEG alpha power and intelligence. Intelligence [Internet]. 2002 May;30(3):289–302. Available from: http://www.sciencedirect.com/science/article/pii/S0160289601001015
25. Klimesch W, Schimke H, Schwaiger J. Episodic and semantic memory: an analysis in the EEG theta and alpha band. Electroencephalogr Clin Neurophysiol. IRELAND; 1994 Dec;91(6):428–41.
26. Klimesch W, Schimke H, Pfurtscheller G. Alpha frequency, cognitive load and memory performance. Brain Topogr [Internet]. 5(3):241–51. Available from: http://dx.doi.org/10.1007/BF01128991
27. Pfurtscheller G. Event-related desynchronization (ERD) during visual processing. Int J Psychophysiol. 1994;16(94):147–53.
28. Lopes da Silva F. Neural mechanisms underlying brain waves: from neural membranes to networks. Electroencephalogr Clin Neurophysiol [Internet]. 1991;79(2):81–93. Available from: http://www.sciencedirect.com/science/article/pii/0013469491900445
29. Lehmann D, Ozaki H, Pal I. EEG alpha map series: brain micro-states by space-oriented adaptive segmentation. Electroencephalogr Clin Neurophysiol [Internet]. 1987 Sep;67(3):271–88. Available from: http://www.ncbi.nlm.nih.gov/pubmed/2441961
30. Lehmann D, Faber PL, Galderisi S, Herrmann WM, Kinoshita T, Koukkou M, et al. EEG microstate duration and syntax in acute, medication-naive, first-episode schizophrenia: a multi-center study. Psychiatry Res [Internet]. 2005 Feb 28 [cited 2013 Feb 4];138(2):141–56. Available from: http://www.ncbi.nlm.nih.gov/pubmed/15766637
31. Nishida K, Morishima Y, Yoshimura M, Isotani T, Irisawa S, Jann K, et al. EEG microstates associated with salience and frontoparietal networks in frontotemporal dementia, schizophrenia and Alzheimer's disease. Clin Neurophysiol [Internet]. International Federation of Clinical Neurophysiology; 2013;124(6):1106–14. Available

from: http://dx.doi.org/10.1016/j.clinph.2013.01.005
32. Khanna A, Pascual-Leone A, Michel CM, Farzan F. Microstates in resting-state EEG: Current status and future directions. Neurosci Biobehav Rev [Internet]. 2015 Feb;49:105–13. Available from: http://www.sciencedirect.com/science/article/pii/S0149763414003492
33. Lehmann D, Strik WK, Henggeler B, Koenig T, Koukkou M. Brain electric microstates and momentary conscious mind states as building blocks of spontaneous thinking: I. Visual imagery and abstract thoughts. Int J Psychophysiol [Internet]. 1998 Jun;29(1):1–11. Available from: http://www.ncbi.nlm.nih.gov/pubmed/9641243
34. Milz P, Faber PL, Lehmann D, Koenig T, Kochi K, Pascual-Marqui RD. The functional significance of EEG microstates—Associations with modalities of thinking. Neuroimage [Internet]. Elsevier Inc.; 2015;125:643–56. Available from: http://linkinghub.elsevier.com/retrieve/pii/S105381191500734X
35. Van Den Heuvel MP, Pol HEH. Exploring the brain network: a review on resting-state fMRI functional connectivity. Eur Neuropsychopharmacol. Elsevier; 2010;20(8):519–34.
36. Damoiseaux JS, Rombouts S, Barkhof F, Scheltens P, Stam CJ, Smith SM, et al. Consistent resting-state networks across healthy subjects. Proc Natl Acad Sci. National Acad Sciences; 2006;103(37):13848–53.
37. Van de Ville D, Britz J, Michel CM. EEG microstate sequences in healthy humans at rest reveal scale-free dynamics. Proc Natl Acad Sci U S A [Internet]. 2010 Oct 19 [cited 2012 Nov 12];107(42):18179–84. Available from: http://www.pubmedcentral.nih.gov/articlerender.fcgi?artid=2964192&tool=pmcentrez&rendertype=abstract
38. Britz J, Van De Ville D, Michel CM. BOLD correlates of EEG topography reveal rapid resting-state network dynamics. Neuroimage [Internet]. Elsevier Inc.; 2010 Oct 1 [cited 2013 Feb 27];52(4):1162–70. Available from: http://www.ncbi.nlm.nih.gov/pubmed/20188188
39. Musso F, Brinkmeyer J, Mobascher a, Warbrick T, Winterer G. Spontaneous brain activity and EEG microstates. A novel EEG/fMRI analysis approach to explore resting-state networks. Neuroimage [Internet]. Elsevier B.V.; 2010 Oct 1 [cited 2012 Nov 2];52(4):1149–61. Available from: http://www.ncbi.nlm.nih.gov/pubmed/20139014
40. Yuan H, Zotev V, Phillips R, Drevets WC, Bodurka J. Spatiotemporal dynamics of the brain at rest - Exploring EEG microstates as electrophysiological signatures of BOLD resting state networks. Neuroimage [Internet]. Elsevier Inc.; 2012;60(4):2062–72. Available from: http://dx.doi.org/10.1016/j.neuroimage.2012.02.031
41. Melnick MD, Harrison BR, Park S, Bennetto L, Tadin D. A Strong Interactive Link between Sensory Discriminations and Intelligence. Curr Biol [Internet]. Elsevier Ltd; 2013;23(11):1–5. Available from: http://dx.doi.org/10.1016/j.cub.2013.04.053\npapers3://publication/doi/10.1016/j.cub.2013.04.053
42. Buschman TJ, Siegel M, Roy JE, Miller EK. Neural substrates of cognitive capacity limitations. Proc Natl Acad Sci U S A. United States; 2011 Jul;108(27):11252–5.
43. Kievit R a, Davis SW, Mitchell DJ, Taylor JR, Duncan J, Henson RN a. Distinct aspects of frontal lobe structure mediate age-related differences in fluid intelligence and multitasking. Nat Commun [Internet]. Nature Publishing Group; 2014;5:5658. Available from: http://www.pubmedcentral.nih.gov/articlerender.fcgi?artid=4284640&tool=pmcentrez&re

ndertype=abstract
44. Gazzaley A, Rissman J, Cooney J, Rutman A, Seibert T, Clapp W, et al. Functional interactions between prefrontal and visual association cortex contribute to top-down modulation of visual processing. Cereb Cortex. United States; 2007 Sep;17 Suppl 1:i125–35.
45. Narr KL, Woods RP, Thompson PM, Szeszko P, Robinson D, Dimtcheva T, et al. Relationships between IQ and regional cortical gray matter thickness in healthy adults. Cereb Cortex. United States; 2007 Sep;17(9):2163–71.
46. Delorme A, Makeig S. EEGLAB: an open source toolbox for analysis of single-trial EEG dynamics including independent component analysis. J Neurosci Methods. Netherlands; 2004 Mar;134(1):9–21.
47. Mognon A, Jovicich J, Bruzzone L, Buiatti M. ADJUST: An automatic EEG artifact detector based on the joint use of spatial and temporal features. Psychophysiology [Internet]. Blackwell Publishing Inc; 2011 Feb 1;48(2):229–40. Available from: http://dx.doi.org/10.1111/j.1469-8986.2010.01061.x
48. Khanna A, Pascual-Leone A, Farzan F. Reliability of resting-state microstate features in electroencephalography. PLoS One. Public Library of Science; 2014;9(12):e114163.
49. Lehmann D. Multichannel topography of human alpha EEG fields. Electroencephalogr Clin Neurophysiol. 1971;31(5):439–49.
50. Brunet D, Murray MM, Michel CM. Spatiotemporal analysis of multichannel EEG: CARTOOL. Comput Intell Neurosci [Internet]. 2011 Jan [cited 2012 Nov 28];2011:813870. Available from: http://www.pubmedcentral.nih.gov/articlerender.fcgi?artid=3022183&tool=pmcentrez&rendertype=abstract
51. Pascual-Marqui RD, Michel CM, Lehmann D. Segmentation of brain electrical activity into microstates: model estimation and validation. IEEE Trans Biomed Eng [Internet]. 1995 Jul;42(7):658–65. Available from: http://www.ncbi.nlm.nih.gov/pubmed/7622149
52. Tibshirani R, Walther G. Cluster Validation by Prediction Strength. J Comput Graph Stat. 2005;14(December 2013):511–28.
53. Koenig T, Prichep L, Lehmann D, Sosa PV, Braeker E, Kleinlogel H, et al. Millisecond by millisecond, year by year: normative EEG microstates and developmental stages. Neuroimage. 2002;16(1):41–8.
54. Raven J, Court JH. Manual for Raven's Progressive Matrices and Vocabulary Scales [Internet]. Oxford Psychologists Press; 1998. Available from: https://books.google.com/books?id=n_AxPwAACAAJ
55. Matzen LE, Benz ZO, Dixon KR, Posey J, Kroger JK, Speed AE. Recreating Raven's: software for systematically generating large numbers of Raven-like matrix problems with normed properties. Behav Res Methods. United States; 2010 May;42(2):525–41.
56. Hossiep R, Turck D, Hasella M. Bochumer Matrizentest-advanced-short version (BOMAT-A). Göttingen: Hogrefe. 2001;
57. Burgess GC, Gray JR, Conway ARA, Braver TS. Neural mechanisms of interference control underlie the relationship between fluid intelligence and working memory span. J Exp Psychol Gen. United States; 2011 Nov;140(4):674–92.
58. Gazzaley A, Cooney JW, Rissman J, D'Esposito M. Top-down suppression deficit underlies working memory impairment in normal aging. Nat Neurosci [Internet]. Nature Publishing Group; 2005 Oct;8(10):1298–300. Available from:

http://dx.doi.org/10.1038/nn1543
59. Gray JR, Thompson PM. Neurobiology of intelligence: science and ethics. Nat Rev Neurosci. Nature Publishing Group; 2004;5(6):471–82.
60. Kaiser HF. The varimax criterion for analytic rotation in factor analysis. Psychometrika [Internet]. 23(3):187–200. Available from: http://dx.doi.org/10.1007/BF02289233
61. Bartlett MS. Properties of Sufficiency and Statistical Tests. Proc R Soc Lond A Math Phys Sci [Internet]. The Royal Society; 1937;160(901):268–82. Available from: http://www.jstor.org/stable/96803
62. Benedek M, Jauk E, Sommer M, Arendasy M, Neubauer AC. Intelligence, creativity, and cognitive control: The common and differential involvement of executive functions in intelligence and creativity. Intelligence [Internet]. Elsevier; 2014 Sep 28;46:73–83. Available from: http://www.ncbi.nlm.nih.gov/pmc/articles/PMC4175011/
63. Dang C-P, Braeken J, Colom R, Ferrer E, Liu C. Why is working memory related to intelligence? Different contributions from storage and processing. Memory. England; 2014;22(4):426–41.
64. Filmer HL, Dux PE, Mattingley JB. Applications of transcranial direct current stimulation for understanding brain function. Trends Neurosci. England; 2014 Dec;37(12):742–53.
65. Santarnecchi E, Brem A-K, Levenbaum E, Thompson T, Kadosh RC, Pascual-Leone A. Enhancing cognition using transcranial electrical stimulation. Curr Opin Behav Sci [Internet]. 2015 Aug;4:171–8. Available from: http://www.sciencedirect.com/science/article/pii/S2352154615000819
66. Michel CM. Electrical Neuroimaging [Internet]. Cambridge University Press; 2009. Available from: https://books.google.com/books?id=LdGn-Jzg0_MC
67. Vakhtin AA, Ryman SG, Flores RA, Jung RE. Functional brain networks contributing to the Parieto-Frontal Integration Theory of Intelligence. Neuroimage. United States; 2014 Dec;103:349–54.
68. Beaujean AA, Firmin MW, Michonski JD, Berry T, Johnson C. A Multitrait—Multimethod Examination of the Reynolds Intellectual Assessment Scales in a College Sample. Assess [Internet]. 2010 Sep 1;17 (3):347–60. Available from: http://asm.sagepub.com/content/17/3/347.abstract
69. COLE JC, LOPEZ BR, DALEO D V. LATENT RELATIONSHIPS OF FLUID, VISUAL, AND SIMULTANEOUS COGNITIVE TASKS. Psychol Rep [Internet]. Ammons Scientific; 2004 Apr 1;94(2):547–61. Available from: http://dx.doi.org/10.2466/pr0.94.2.547-561
70. Conway ARA, Cowan N, Bunting MF, Therriault DJ, Minkoff SRB. A latent variable analysis of working memory capacity, short-term memory capacity, processing speed, and general fluid intelligence. Intelligence [Internet]. 2002 Mar;30(2):163–83. Available from: http://www.sciencedirect.com/science/article/pii/S0160289601000964
71. Crone EA, Wendelken C, van Leijenhorst L, Honomichl RD, Christoff K, Bunge SA. Neurocognitive development of relational reasoning. Dev Sci. England; 2009 Jan;12(1):55–66.
72. Perfetti B, Saggino A, Ferretti A, Caulo M, Romani GL, Onofrj M. Differential patterns of cortical activation as a function of fluid reasoning complexity. Hum Brain Mapp. United States; 2009 Feb;30(2):497–510.
73. Yuan Z, Qin W, Wang D, Jiang T, Zhang Y, Yu C. The salience network contributes to an individual's fluid reasoning capacity. Behav Brain Res. Netherlands; 2012

Apr;229(2):384–90.
74. Martinez A, Anllo-Vento L, Sereno MI, Frank LR, Buxton RB, Dubowitz DJ, et al. Involvement of striate and extrastriate visual cortical areas in spatial attention. Nat Neurosci. UNITED STATES; 1999 Apr;2(4):364–9.
75. Bondarenko R, Boehler CN, Stoppel CM, Heinze H-J, Schoenfeld MA, Hopf J-M. Separable mechanisms underlying global feature-based attention. J Neurosci. United States; 2012 Oct;32(44):15284–95.
76. Peters JC, Roelfsema PR, Goebel R. Task-relevant and accessory items in working memory have opposite effects on activity in extrastriate cortex. J Neurosci. United States; 2012 Nov;32(47):17003–11.
77. Carpenter PA, Just MA, Shell P. What one intelligence test measures: a theoretical account of the processing in the Raven Progressive Matrices Test. Psychol Rev. UNITED STATES; 1990 Jul;97(3):404–31.
78. Micheloyannis S, Pachou E, Stam CJ, Vourkas M, Erimaki S, Tsirka V. Using graph theoretical analysis of multi channel EEG to evaluate the neural efficiency hypothesis. Neurosci Lett. Ireland; 2006 Jul;402(3):273–7.
79. Neubauer AC, Fink A. Intelligence and neural efficiency. Neurosci Biobehav Rev. United States; 2009 Jul;33(7):1004–23.
80. Santarnecchi E, Galli G, Polizzotto NR, Rossi A, Rossi S. Efficiency of weak brain connections support general cognitive functioning. Hum Brain Mapp [Internet]. 2014 Sep 1;35(9):4566–82. Available from: http://dx.doi.org/10.1002/hbm.22495
81. Neubauer AC, Grabner RH, Freudenthaler HH, Beckmann JF, Guthke J. Intelligence and individual differences in becoming neurally efficient. Acta Psychol (Amst). Netherlands; 2004 May;116(1):55–74.
82. Malhotra P, Coulthard EJ, Husain M. Role of right posterior parietal cortex in maintaining attention to spatial locations over time. Brain [Internet]. 2009 Apr 1;132(3):645–60. Available from: http://brain.oxfordjournals.org/content/132/3/645.abstract
83. Verney SP, Granholm E, Marshall SP, Malcarne VL, Saccuzzo DP. Culture-Fair Cognitive Ability Assessment: Information Processing and Psychophysiological Approaches . Assess [Internet]. 2005 Sep 1;12 (3):303–19. Available from: http://asm.sagepub.com/content/12/3/303.abstract
84. Kush JC, Spring MB, Barkand J. Advances in the assessment of cognitive skills using computer-based measurement. Behav Res Methods. United States; 2012 Mar;44(1):125–34.
85. Basar E. A review of alpha activity in integrative brain function: fundamental physiology, sensory coding, cognition and pathology. Int J Psychophysiol. Netherlands; 2012 Oct;86(1):1–24.
86. Klimesch W. Alpha-band oscillations, attention, and controlled access to stored information. Trends Cogn Sci [Internet]. Elsevier Science; 2012 Dec;16(12):606–17. Available from: http://www.ncbi.nlm.nih.gov/pmc/articles/PMC3507158/
87. Oelhafen S, Nikolaidis A, Padovani T, Blaser D, Koenig T, Perrig WJ. Increased parietal activity after training of interference control. Neuropsychologia. Elsevier; 2013;51(13):2781–90.
88. Houdé O, Zago L, Mellet E, Moutier S, Pineau A, Mazoyer B, et al. Shifting from the perceptual brain to the logical brain: The neural impact of cognitive inhibition training. J Cogn Neurosci. MIT Press; 2000;12(5):721–8.

89. Aron AR, Robbins TW, Poldrack RA. Inhibition and the right inferior frontal cortex: one decade on. Trends Cogn Sci. England; 2014 Apr;18(4):177–85.
90. Prado J, Noveck IA. Overcoming perceptual features in logical reasoning: A parametric functional magnetic resonance imaging study. J Cogn Neurosci. 2007;19(4):642–57.
91. Prado J, Kaliuzhna M, Cheylus A, Noveck IA. Overcoming perceptual features in logical reasoning: An event-related potentials study. Neuropsychologia. Pergamon; 2008;46(11):2629–37.
92. Baker AP, Brookes MJ, Rezek IA, Smith SM, Behrens T, Probert Smith PJ, et al. Fast transient networks in spontaneous human brain activity. Culham JC, editor. Elife [Internet]. 2014 Mar 25;3. Available from: http://elifesciences.org/content/3/e01867.abstract
93. Haier RJ. Increased intelligence is a myth (so far). Front Syst Neurosci [Internet]. Frontiers Media S.A.; 2014 Mar 12;8:34. Available from: http://www.ncbi.nlm.nih.gov/pmc/articles/PMC3950413/
94. Murray MM, Brunet D, Michel CM. Topographic ERP analyses: a step-by-step tutorial review. Brain Topogr [Internet]. 2008 Jun [cited 2012 Oct 28];20(4):249–64. Available from: http://www.ncbi.nlm.nih.gov/pubmed/18347966
95. Stam CJ. Nonlinear dynamical analysis of EEG and MEG: review of an emerging field. Clin Neurophysiol. Elsevier; 2005;116(10):2266–301.
96. Crutchfield JP, Packard NH. Symbolic dynamics of noisy chaos. Phys D Nonlinear Phenom. Elsevier; 1983;7(1):201–23.
97. Davidchack RL, Lai Y, Bollt EM, Dhamala M. Estimating generating partitions of chaotic systems by unstable periodic orbits. Phys Rev E [Internet]. 2000;61(2):1353–6. Available from: http://link.aps.org/doi/10.1103/PhysRevE.61.1353
98. So P, Francis JT, Netoff TI, Gluckman BJ, Schiff SJ. Periodic orbits: a new language for neuronal dynamics. Biophys J [Internet]. Elsevier; 1998 Jun [cited 2013 Jul 25];74(6):2776–85. Available from: http://www.pubmedcentral.nih.gov/articlerender.fcgi?artid=1299619&tool=pmcentrez&rendertype=abstract
99. Zoldi SM, Greenside HS. Spatially Localized Unstable Periodic Orbits. 1997;1–16.
100. So P, Ott E, Schiff SSJ, Kaplan DTD, Sauer T, Grebogi C. Detecting unstable periodic orbits in chaotic experimental data. Phys Rev Lett [Internet]. American Physical Society; 1996 Jun 17;76(25):4705–8. Available from: http://link.aps.org/doi/10.1103/PhysRevLett.76.4705
101. So P, Ott E, Sauer T, Gluckman BJ, Grebogi C, Schiff SJ. Extracting unstable periodic orbits from chaotic time series data. Phys Rev E [Internet]. 1997 May;55(5):5398–417. Available from: http://link.aps.org/doi/10.1103/PhysRevE.55.5398
102. Bradley E, Mantilla R. Recurrence plots and unstable periodic orbits. Chaos [Internet]. 2002 Sep [cited 2013 Jul 29];12(3):596–600. Available from: http://www.ncbi.nlm.nih.gov/pubmed/12779588
103. Schmelcher P, Diakonos F. Detecting Unstable Periodic Orbits of Chaotic Dynamical Systems. Phys Rev Lett [Internet]. 1997 Jun;78(25):4733–6. Available from: http://link.aps.org/doi/10.1103/PhysRevLett.78.4733
104. Zou Y, Donner R V., Donges JF, Marwan N, Kurths J. Identifying complex periodic windows in continuous-time dynamical systems using recurrence-based methods. Chaos. 2010;20(4):7–9.

105. Gottfredson LS. Intelligence: Is it the epidemiologists' elusive "fundamental cause" of social class inequalities in health? J Pers Soc Psychol. 2004;86(1):174–99.

VII. TABLES & FIGURES

Note: These tables and figures have been submitted for publication in:
Santarnecchi E, Khanna AR, Museus C, Benwell C, Davila P, Pascual-Leone A, Shafi MM. EEG microstate correlates of fluid intelligence and response to cognitive training. Proceedings of the National Academy of Science (Submitted, under review); 2016.

TABLE 1: Microstate properties. Average values and standard deviation for each microstate feature extracted from the overall sample at baseline is reported. Values grouped around three categories, related to (i) the intrinsic characteristic of each microstate, the (ii) dynamic transition between each pair of states, (iii) overall properties referred to the state space with no reference to specific states.

Microstates properties	**Mean**	**Standard Deviation**
Avg Life A	48.84	7.27
Avg Life B	48.53	7.23
Avg Life C	50.46	7.70
Avg Life D	60.83	8.53
Freq A	4.19	1.14
Freq B	3.91	1.31
Freq C	3.36	.50
Freq D	5.14	.77
Coverage A	21.24	7.43
Coverage B	19.91	7.94
Coverage C	20.97	7.98
Coverage D	37.88	13.55
GFP Peaks/Appear A	1.31	.13
GFP Peaks/Appear B	1.29	.12
GFP Peaks/Appear C	1.32	.15
GFP Peaks/Appear D	1.85	1.24
Transitions		
A → B	.27	.11
A → C	.27	.09
A → D	.45	.13
B → A	.29	.10
B → C	.26	.09
B → D	.45	.13
C → A	.28	.09
C → B	.26	.10
C → D	.47	.15
D → A	.34	.10
D → B	.31	.10
D → C	.35	.13
Global Scores		
Global Avg Life	58.26	15.79
Global Freq	17.78	2.55
Global GFP Peaks/sec	26.27	2.26

TABLE 2: Correlation between microstate properties and *Gf* scores. Pearson product-moment coefficient, as well as p.values, for the correlation between microstate properties and *Gf-1* and Gf-2 individual scores are shown. (*) and (**) respectively highlight statistically significant correlations at $p<0.05$ and $p<0.01$.

		Gf 1	Gf 2
State properties			
Avg Life A	*corr coeff*	0.016	-0.096
	p.value	0.867	0.313
Avg Life B		0.094	-0.081
		0.325	0.397
Avg Life C		-0.089	0.036
		0.349	0.705
Avg Life D		.189*	0.033
		0.046	0.726
Freq A		-0.163	-0.147
		0.085	0.121
Freq B		-0.031	**-0.346 (*)**
		0.745	**0.012**
Freq C		**-0.503 (**)**	-0.132
		0.002	0.136
Freq D		0.126	-0.114
		0.186	0.232
Coverage A		-0.131	-0.099
		0.169	0.300
Coverage B		0.008	-0.101
		0.933	0.288
Coverage C		0.022	0.048
		0.821	0.616
Coverage D		0.048	0.071
		0.613	0.459
GFP Peaks/Appear A		-0.181	-0.059
		0.057	0.539
GFP Peaks/Appear B		-0.039	-0.056
		0.683	0.557
GFP Peaks/Appear C		0.019	-0.014
		0.840	0.887
GFP Peaks/Appear D		-0.073	0.113
		0.442	0.237
Global Scores			
Global Avg Life	*corr coeff*	0.012	0.077
	p.value	0.901	0.419
Global Freq		-0.107	-0.071
		0.261	0.457
Global GFP Peaks/sec		-0.451	0.086
		0.008	0.367

		Gf 1	Gf 2
Transitions			
A → B	*corr coeff*	-0.014	**-0.281 (*)**
	p.value	0.884	**0.019**
A → C		-0.030	0.048
		0.751	0.613
A → D		0.036	0.029
		0.709	0.763
B → A		-0.164	-0.102
		0.084	0.285
B → C		0.024	0.043
		0.798	0.654
B → D		0.091	0.031
		0.340	0.742
C → A		-0.174	-0.089
		0.066	0.353
C → B		-0.006	-0.095
		0.948	0.320
C → D		0.109	0.116
		0.251	0.221
D → A		-0.126	-0.115
		0.186	0.227
D → B		0.078	**-0.279 (*)**
		0.411	**0.018**
D → C		0.034	0.174
		0.725	0.066

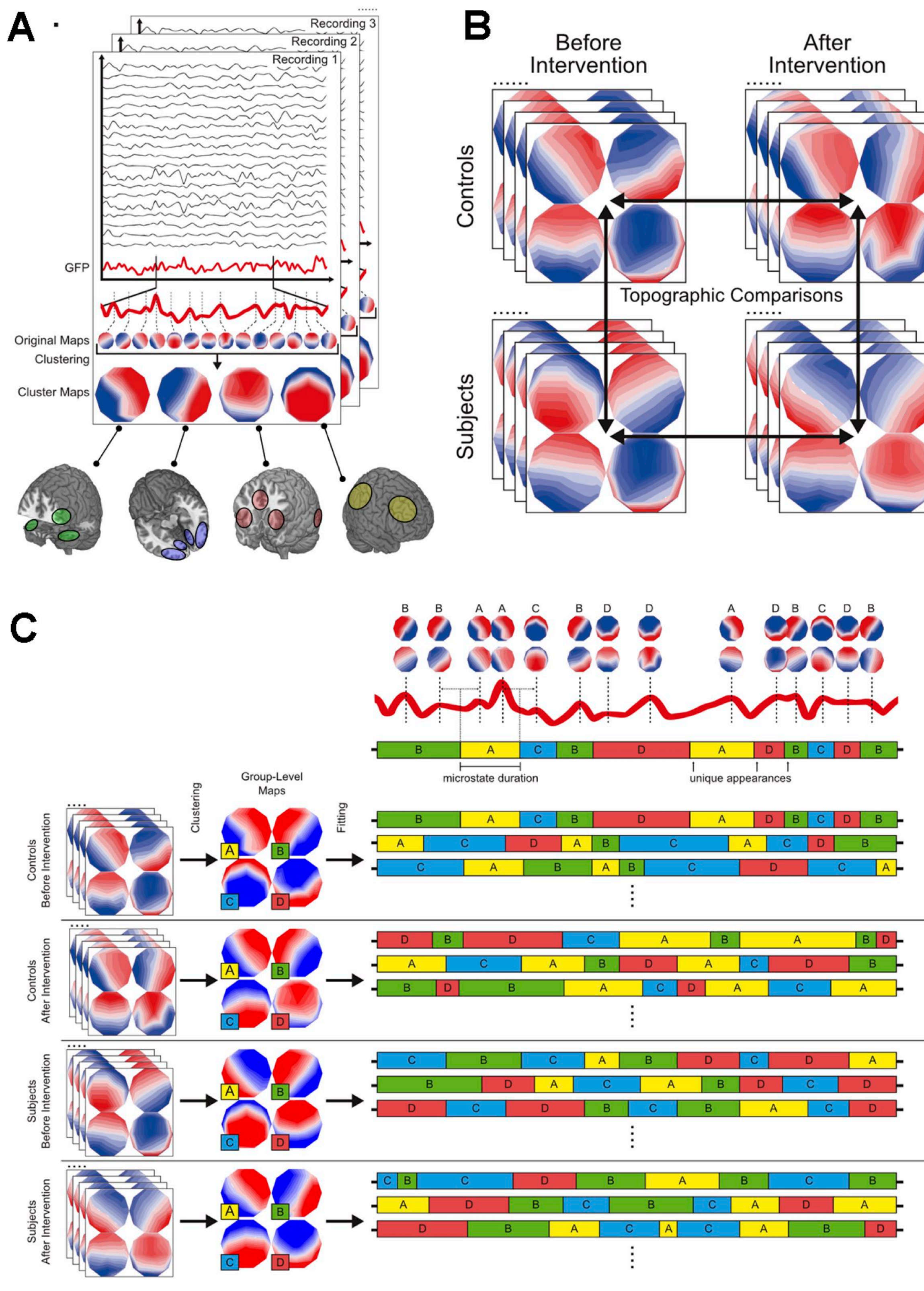
A
Recording 3
Recording 2
Recording 1
GFP
Original Maps
Clustering
Cluster Maps
B
Before Intervention
After Intervention
Controls
Subjects
Topographic Comparisons
C
microstate duration
unique appearances
Group-Level Maps
Clustering
Fitting
Controls Before Intervention
Controls After Intervention
Subjects Before Intervention
Subjects After Intervention

FIGURE 1: Schematic overview of the method of EEG microstate analysis. (A) Each individual EEG recording is initially individually analyzed. First, the GFP at each time point is calculated and plotted to construct a GFP curve for each recording (red). Maps at local maxima of the GFP curve represent instances of highest topographic signal-to-noise ratio and are reliable topographic representations of surrounding points in time; therefore, they are selected for further analysis. The maps at all local maxima of the GFP curve are identified as “original maps.” All original maps from each recording are submitted to a clustering algorithm individually, and four cluster maps are generated for each individual recording. (B) The four cluster maps generated for each individual recording are used to conduct topographic analysis of variance (TANOVA) to assess for topographic differences in any microstate class across groups or conditions. (C) Cluster maps generated for each individual recording are grouped according to group and condition. Maps in each group are submitted to another round of clustering to generate a set of 4 group-level maps for each group. These group-level maps are fit onto the original data by labeling each original map A, B, C, or D depending on which group-level map it most closely correlates to. Each original recording is ultimately re-expressed as a sequence of these labels, from which values of interest can be calculated. Note that only the map's topography is important, whereas polarity is disregarded in the spontaneous EEG clustering algorithm.

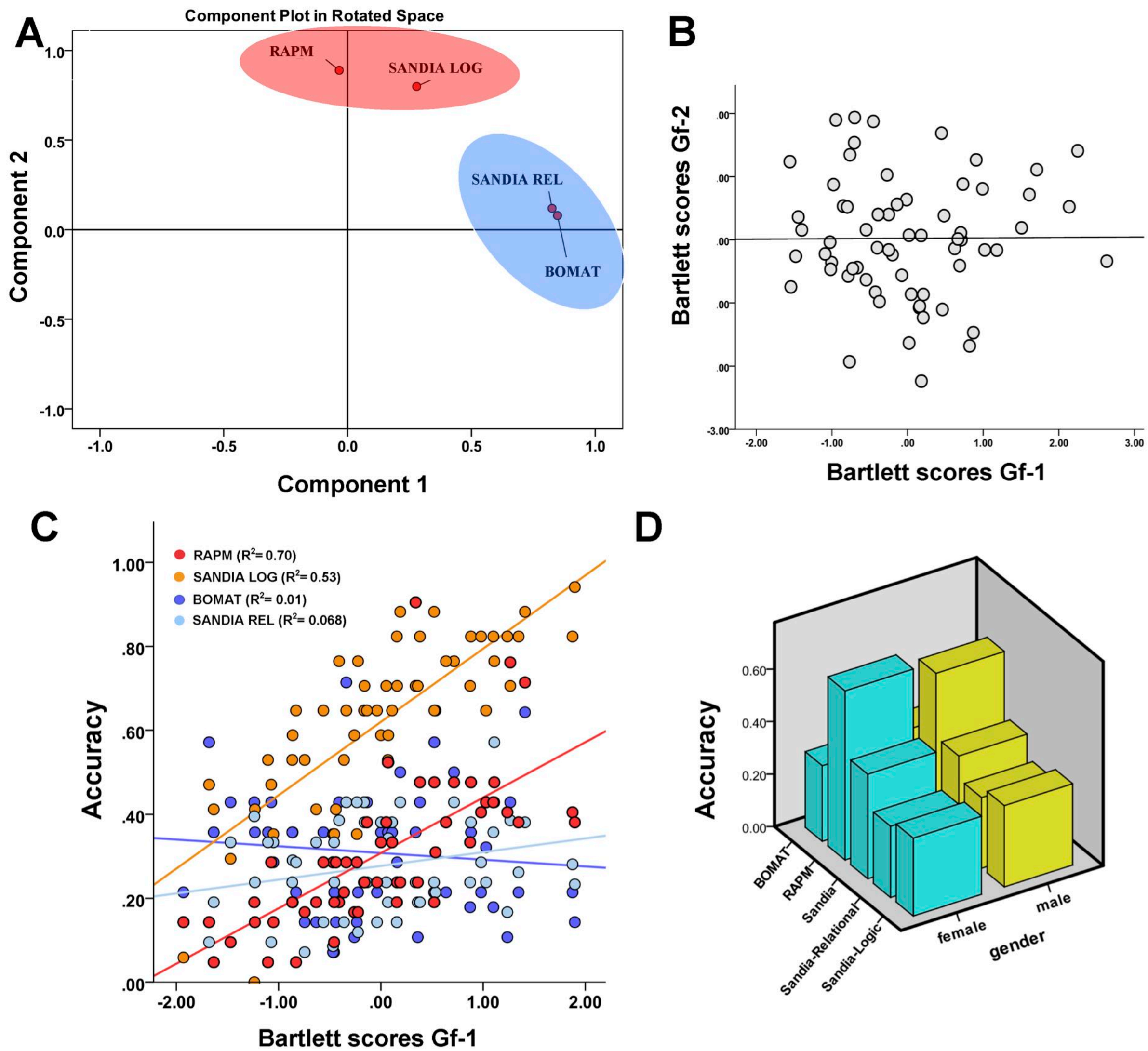

FIGURE 2. Fluid intelligence components at the latent variable level. Panel (A) shows the loading of each *Gf* task in the rotated space obtained using PCA, with the two components highlighted in red and blue, respectively. (B) Resulting individual Bartlett scores for the PCA components show good statistical separation of the two *Gf* components (Pearson "r" coefficient is close to 0). (C) Correlations between *Gf-1* and accuracy levels for each *Gf* task show that *Gf-1* loads primarily on RAPM and Sandia-LOG at baseline (red and orange dots, respectively). (D) Mean scores for the fluid intelligence tasks show no gender related differences. Note: all straight lines represent a linear fit for the different data, with the percentage of explained variance reported using R squared values.

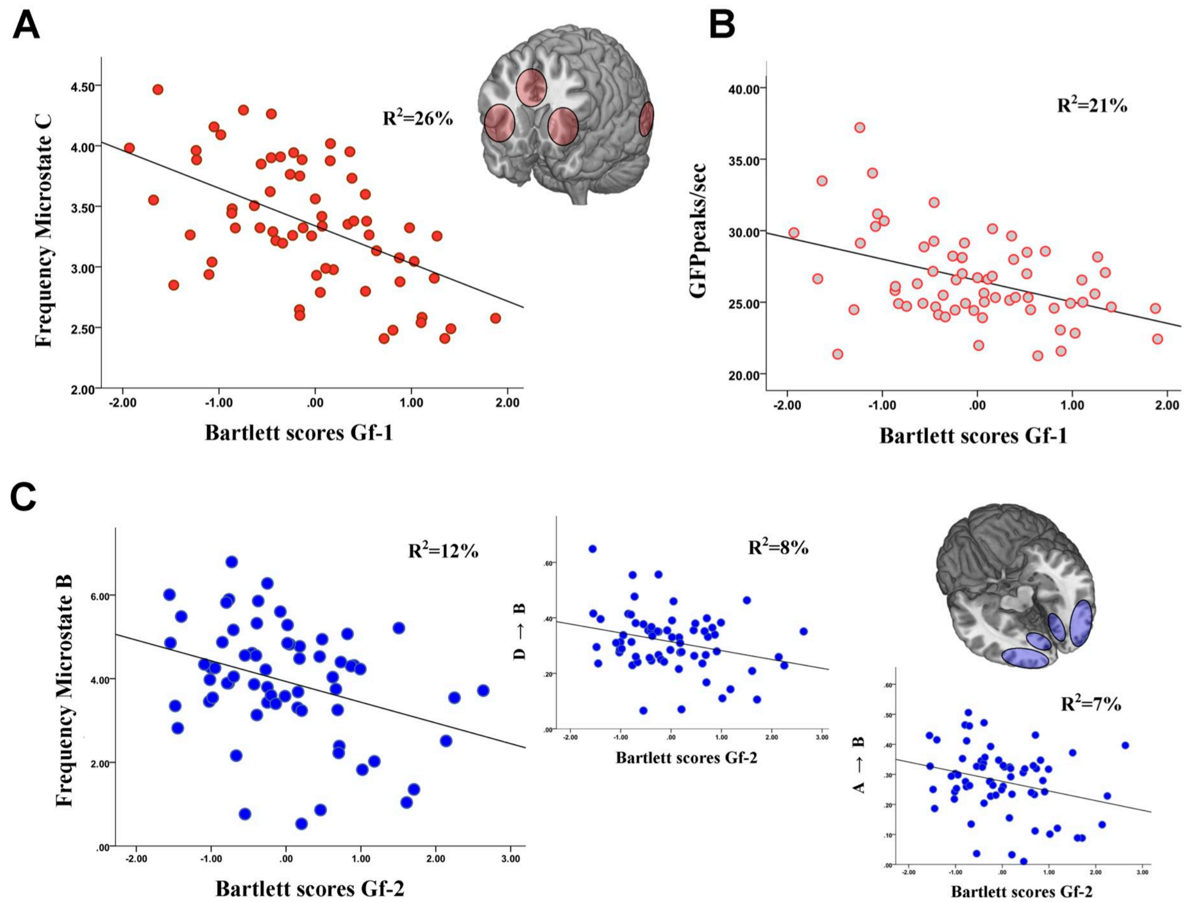

FIGURE 3. Baseline correlation of fluid intelligence with microstate features. (A) Significant negative correlation between Bartlett scores derived for the first component (*Gf-1*) and the frequency of appearance of microstates C. (B) *Gf-1* also showed a significant negative correlation with the number of GFP peaks per sec. (C) Significant correlations between Bartlett scores for *Gf-2* and the frequency of microstate B, as well as with the probability of transition from state A and D towards microstate B. Note: straight lines represent a linear fit for the different data, with the percentage of explained variance reported using R squared values. 3D brains show a schematic view of the anatomo-functional localization of microstates B and C as reported in Britz et al. 2010 (38).

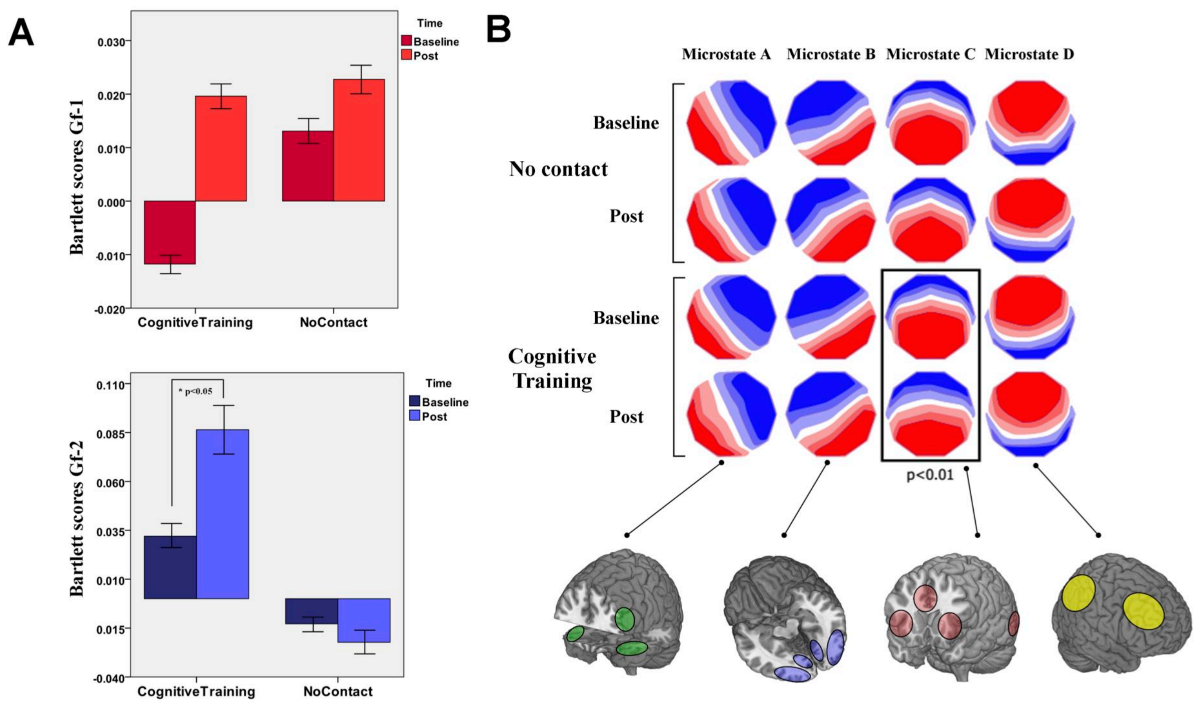

FIGURE 4: Behavioral and Topographic differences before and after intervention in controls and trained subjects. Panel (A) reports the comparisons between the Bartlett scores for the two *Gf* factors calculated before and after the intervention in the two groups. A significant effect of cognitive training is observed for *Gf-2* in the cognitive training group (*). (B) Original maps at local maxima of the GFP curve for each EEG recording were submitted to a topographic clustering algorithm to derive four representative microstate maps for each recording. Maps in each set of four were labeled A, B, C, and D depending on their topographic correlation with the "archetypal" microstates A, B, C, and D that have been described in numerous prior studies. These sets of maps from individual EEG recordings were compared using the topographic analysis of variance (TANOVA) randomization statistical test. The microstates A, B, C, and D shown for each group represent electrode-by-electrode averages of all microstates of the given class within each group. TANOVA revealed a significant difference in the topography of microstate C after cognitive training ($p<0.01$). No other significant topographic differences were identified. Note: 3D brains show a schematic view of the anatomo-functional localization of microstates B and C as reported in Britz et al. 2010 (38).

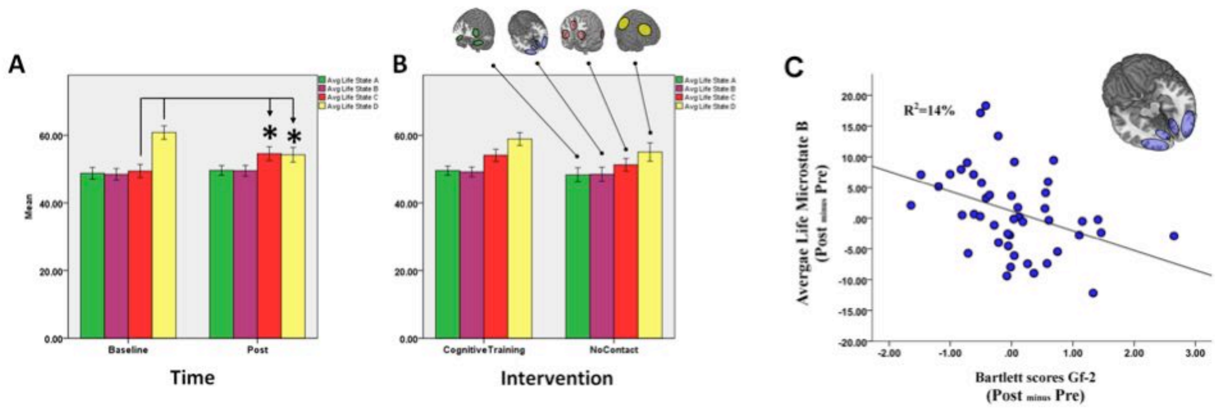

FIGURE 5: Training effects on microstates properties. Panel (A) and (B) report results of the repeated-measures-ANCOVA run on the average lifespan values of each microstate class. The only significant results were related to the effect of TIME on the average lifespan of microstate C and D (*), with no significant differences between participants in the cognitive training and no-contact group. No significant results were identified for the interaction between TIME and INTERVENTION, as well as for the remaining microstates properties (e.g. frequency, coverage, GFP peaks). (C) Scatterplot displays the negative correlation between changes in microstates properties and fluid intelligence scores after training, with the average life of state B being inversely correlated with changes in *Gf-2* in the group receiving cognitive training. No other correlation coefficients reached the significance level (p<0.05 Bonferroni corrected for multiple comparisons).